NTNU
Norwegian University of
Science and Technology

State Estimation with Wave Filtering for an Unmanned Surface Vehicle

by utilizing acceleration feedback

Kåre Andreas Nystad Jørgensen

Master of Science in Engineering Cybernetics
Submission date: June 2011
Supervisor: Tor Arne Johansen, ITK

Norwegian University of Science and Technology
Department of Engineering Cybernetics

Problem Description

The task is about observers for dynamic positioning of small vessels, including docking and weathervaning. Waves might affect small vessels considerably, and the challenge is to compensate for these disturbances in the control system. High-frequency wave motion is commonly filtered out of the measurement because counteracting this motion would be useless, and would only lead to excessive wear and tear. For small vessels however, it is assumed that this motion has to be compensated for by the thrusters and propellers.

The main objective is to compare the performance of an observer for dynamic positioning that utilizes a vessel model, with a navigation-type observer that does not utilize a vessel model. In both cases, the observers may utilize position, heading and acceleration measurement.

Sub tasks

- Implement a nonlinear model based observer, which can utilize position, heading and acceleration measurements to estimate the states. This observer should be able to choose what level of wave filtering should be done, depending on operational mode and weather.
- Implement a model-free observer that makes use of the measured acceleration as input to generate estimates. This observer should also be able to choose the level of wave filtering, depending on operational mode and weather.
- Compare the above observers in simulations and evaluate the results. Thorough tuning that accounts for the sensors, thrusters and the characteristics of the boat should be carried out.

Assignment given: 25. January 2011

Supervisor: Tor Arne Johansen, ITK

Co-Supervisor: Vegard Evjen Hovstein, Maritime Robotics

Preface

"Once we accept our limits, we go beyond them"

-Albert Einstein

This thesis is the final chapter in my life as a student. It concludes five years at the Norwegian University of Technology and Science, five years that have been a journey through knowledge and experience. I have learned and experienced more than I ever could have imagined, and I am forever grateful of these five years. This thesis have been frustrating and difficult at times, but it has also motivated me for the challenges a head and prepared me for new adventures. Because of these years in Trondheim I will always Cherish the art of learning.

I wish to thank all the people that have contributed to this thesis. Especially my supervisor Tor Arne Johansen for his knowledge and excellent guidance, and Øyvind Kåre Kjerstad for developing a fantastic Viknes simulator and DP system. I also want to express my gratitude to the guys at Maritime Robotics, Vegard Evjen Hovstein, for giving me this assignment and for letting me work with their boat. And of course, I want to thank my fellow students and friends for making it fun and rewarding coming to the office every morning. And last, but not least, I want to thank my girlfriend for being patient and understanding, and for reading and correcting this thesis.

My work on this thesis is now concluded, but I hope that my work here might someday be useful for others working on similar tasks.

Kåre Andreas Nystad Jørgensen

Trondheim, 09/05/11

Abstract

This thesis considers two different state estimators for an unmanned surface vehicle owned by Maritime Robotics. They will both be tested together with a dynamic positioning system developed especially for the vessel in question. The observers should utilize measured acceleration delivered from an IMU, and some kind of wave filtering should be done on the estimates. The emphasis will be put on how good the achieved state estimates are, and on to what degree of wave filtering should be done to the estimates, considering they are meant for a small vessel. Both observers were tested in a Matlab/Simulink dynamic positioning simulator. Two simulation scenarios were used in the simulations, each with different weather conditions.

The first observer was originally an attitude observer which was simplified specifically for this application. It makes use of the measured body-fixed acceleration as input and has feedback from position, heading and velocity. The simulation results turned out to be less than satisfying, but the observer showed potential and could be further developed. The second observer considered was based on a model of the Viknes 830. Instead of using the measured acceleration as input, the measurements were used as feedback to improve the model estimates. This observer performed better than expected in the simulations, reducing both convergence time and controller usage. The simulation results for this observer also indicated that wave filtering could be beneficial for small vessels.

Contents

List of Figures

List of Tables

Abbreviations

AFB - Acceleration Feedback

CDGPS - Carrier Differential Global Positioning System

CG - Center of Gravity

DGPS - Differential Global Positioning System

DOF - Degree Of Freedom

DP - Dynamic Positioning

ECEF - Earth Centered Earth Fixed

ECI - Earth Centered Inertial

GPS - Global Positioning System

IMU - Inertial Measurement Unit

INS - Inertial Navigation System

LF - Low-Frequency

MER - Mars Exploration Rover

NED - North East Down

UAV - Unmanned Aerial Vehicle

UGES - Uniform Global Exponential Stability

USV - Unmanned Surface Vehicle

WF - Wave-Frequency

WOHC - Weather Optimal Heading Control

WOPC - Weather Optimal Positioning Control

Chapter 1

Introduction

1.1 Motivation

These days people are surrounded by all kinds of technology. Technology that often helps people to solve a large number of every day tasks, that otherwise would be to time-consuming or even impossible to do. Different kinds of automated systems are examples of such technology. Most automated systems are made to relieve humans of some kind of work, or even do work that is unsuited for humans. Examples of such tasks are the exploration of Mars with the Mars Exploration Rovers (MERs) and the use of unmanned aerial vehicles (UAVs) for reconnaissance and surveillance missions. While humans easily gets bored and tired, the machines never complain about their tasks. They set out to do the task they are assigned to do, no matter how hard, boring or dangerous it is. For this reason there has been a lot of research on unmanned vessels in the later years. These are vessels that operate autonomously in any kind of environment without human interaction. One kind of unmanned vessel is the unmanned surface vehicle (USV). The USV is a craft that operates on or in the near vicinity of the ocean surface. The research on this kind of vessels have resulted in a small number of experimental crafts that is getting closer to the goal of being completely autonomous, capable of performing simple human ordered tasks. In the near future these vessels are intended to help out in a variety of marine operations stretching from simple reconnaissance and surveillance missions, to rescue operations.

Figure 1.1: A military UAV.

The concept of an unmanned surface vehicles originated at MIT in the early 90's, and was then a simple scale replica of a fishing trawler. In the beginning the development of the USV were limited to research project at various scientific institutions, but in the last decade the development of the global positioning system (GPS) and the increased interest in the concept from the military have accelerated the development of the USV. Today, advanced USVs developed by the US military have been used in several military operations, but the USV have yet to prove its potential commercially. The USV projects of Maritime Robotics aims to develop USVs for commercial use. Especially with large offshore activity in the North Sea, a commercially available USV could prove to be an important contribution to the offshore operations. Potentially the USV could be used for service and inspection tasks both for the offshore oil and gas industry, but also for the emerging ocean-wind and wave power industry. Other tasks could be mapping of the seabed, and a group of USVs could could work together and function as a mooring system for larger installations. To perform these various tasks, the USV has to be fitted with different systems. Guidance and motion control, and dynamic positioning (DP) are examples of such systems.

In DP operation a vessel should be able to hold its position while being affected by external forces such as wind, waves and ocean currents. This thesis will explore the use of measured acceleration to improve the positioning capabilities of the DP system. The measured acceleration will be utilized in an observer to investigate if

the state estimation can be improved. In addition, it will be interesting to explore how wave filtering can be integrated in the state estimation, and how this will affect the performance and station keeping abilities of the DP system.

Figure 1.2: The Mariner USV owned by Maritime Robotics.

1.2 Dynamic Positioning Systems

Dynamic positioning is a widely researched topic in the maritime community, and there have been written dozens of papers and articles on the topic. The idea of having a ship maintain its position at sea while external forces are acting on it have been around for a long time. In the beginning, mooring systems were the only alternative, but cumbersome anchor systems made the positioning operation difficult. The first actual DP vessel with positioning and heading control was fitted with a simple analogue control system interfaced by a taut wire reference. The vessel was equipped with thrusters fore and aft in addition to its main propulsion. The growth and evolution of the offshore oil and gas industry over the past decades have created a whole new set of requirements. Today offshore operations are conducted on deeper water and in more demanding weather than earlier. In addition, there is an increasing attention to environmental friendly operations, which puts additional requirements on the systems that are operating offshore. This has in turn led to great development of the DP technology. By the late 1970s DP had

become a well established technique, and the number of DP capable vessels were increasing.

In Holvik (1998) DP is defined as:

"A means of holding a vessel in relatively fixed position with respect to the ocean floor, without using anchors accomplished by two or more propulsive devices controlled by inputs from sonic instruments on the sea bottom and on the vessel, by gyro compass, by satellite navigation or by other means."

For a vessel to have full DP capabilities it needs to be fully actuated, it needs to allow individual movement in surge, sway and yaw simultaneously. For a small vessel, the size can sometimes constrain the thruster configuration . To avoid confusion when discussing actuation levels on different vessels, Kjerstad (2010) uses two necessary definitions.

Definition 1 *A fully actuated control scheme can be defined as control of n independent states with m inputs, where* $m \geq n$*. If this does not hold the scheme is regarded as under actuated.*

Definition 2 *An under actuated vessel can be defined as the lack of ability to independently control surge, sway and yaw simultaneously.*

A DP system relies on accurate sensor measurements to be able to calculate the needed thrust to the different actuators in order to keep the vessel at the desired position. The different measurements are delivered by the navigation system to the controller and reference model. In the following sections, the control system, the navigation system and the reference model will be discussed. Figure 1.2 shows the different parts of a conventional DP system.

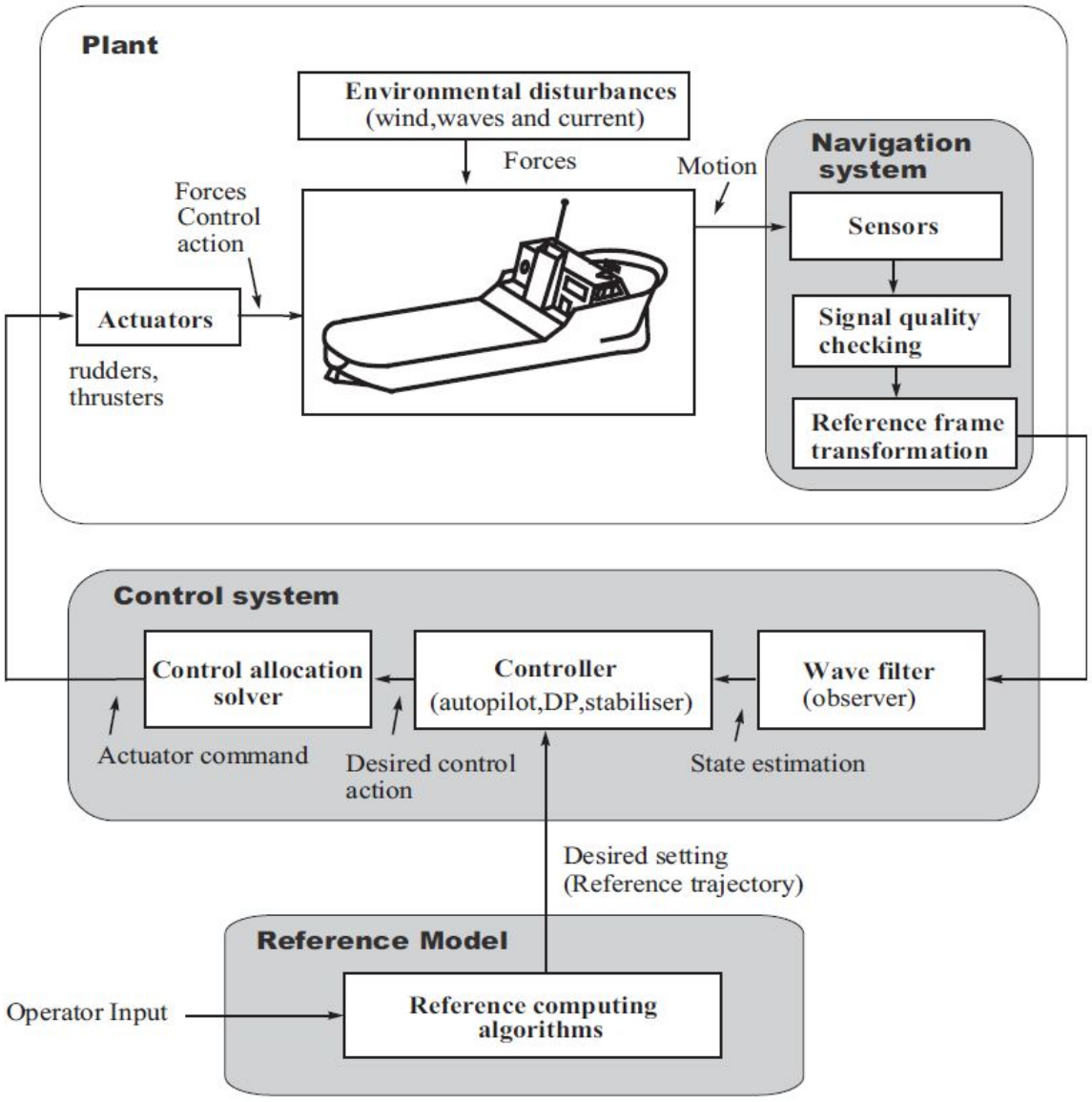

Figure 1.3: A schematic illustration of a modern DP system.

1.2.1 Navigation System

Most control systems requires some kind of measurements to function properly, this is also true for a dynamic positioning system. The navigation system is the

set of all sensors delivering measurements about the state of the vessel. In addition, the navigation system also handles signal processing and reference frame transformation if that is needed.

One of the main problems with DP in the early days was the difficulties of getting reliable and accurate real-time positioning measurements. In order for a DP system to counteract disturbances on the ocean surface it requires continuous measurements of the states of the vessel. Position and state measurements can be obtained through a range of different sensor systems. For highly advanced DP vessels, global positioning systems (GPS) and inertial navigation systems (INS) are the most commonly used systems as these are applicable without a need for additional equipment.

A GPS system relies on satellites to calculate the position. A minimum of 3 satellites are required for the calculation. By utilizing base station with known position, the GPS can be extended to differential GPS (DGPS) or Carrier DGPS (CDGPS) to enhance the accuracy of the position measurement. The GPS measurements are delivered in the earth-centered-earth-fixed (ECEF)-frame, either as Cartesian coordinates or longitude and latitude.

An INS utilizes accelerometers and gyroscopes to measure inertial movement of the vessel. The measurements are given in the body-frame. Each degree of freedom (DOF) has an accelerometer to measure linear acceleration, and each axis has a gyroscope to measure angular velocity about the axis. The INS has to be initialized in order to calculate position and velocity. For a more thorough discussion of navigation and measurement systems see Vik (2010).

Other solutions also exists, for instance hydro acoustic positioning and taut-wire positioning both relies on devices placed on the ocean floor. Laser and microwaves are other alternatives, each with different advantages and disadvantages regarding cost and reliability.

1.2.2 Control System and Reference Model

The measurements taken by the different sensors in the navigation system is delivered to the control system after signal processing and frame transformation. The observer is the first instance of the control system. The observer combines all the available measurements and filters them for noise. Most observers today also includes some kind of wave filter in order to filter out high frequency wave motion. Another feature of the observer is that it provides estimates of states that are difficult to measure i.e. linear velocity. A requirement posed by the classification societies is that the observer must also be able to handle dead-reckoning, which means that the observer must be able to provide estimates of any state if the measurement of that state should drop out for some reason.

For the vessel to get to the desired position in a smooth matter, a reference model is needed. This model delivers a smooth trajectory towards the desired position, avoiding large steps in commanded thrust to the actuators. Along with the measured motion of the vessel, this trajectory is fed to a controller that calculates the body-frame thrust necessary for the vessel to follow the trajectory towards the position set-point. The thrust needed can be calculated in a number of ways, ranging from simple PID controllers to more advanced nonlinear optimization schemes. The last instance of the control system is the thrust allocation scheme. Because different vessels have different thruster configurations and thrusters with different dynamics, the thrust forces calculated by the controller needs to be transformed into set-points that can be interpreted by the thrusters.

DP systems range from very simple to highly sophisticated. The difference often lie in how well the environmental disturbances is handled. In calm easy weather the difference might not be noticeable, but in strong winds and high waves the nonlinearities become more significant, and simple DP systems might not be able to handle them. In addition, the more sophisticated DP systems can be fitted with different operational modes to meet marked demands. Examples of such modes are wind feed-forward, switching between manual, semi-automatic and automatic operational mode. In addition, the increasing focus on environmental operations have led to development of more environmental friendly DP systems.

1.3 Small Vessel Aspects

When applying the DP technology to smaller vessel, some considerations has to be taken. Unlike the large vessel conventional DP systems are designed for, the USVs have a low inertia and a relative small size compared to the waves. This makes them behave very differently at sea. Weather conditions that for larger vessels are negligible, can for a USV induce violent motions in all DOFs. On larger vessel, these motion are normally dampened by the size and inertia of the vessel, and can be filtered out as noise. This reduces wear and tear on the actuators and lowers the fuel consumption. On a USV this might not be as beneficial. A common assumption is that for a small vessel to be able to maintain a position, the high frequency wave motion can not be filtered out. In other words, the oscillatory motion of the waves has to be counteracted by the actuators. This thesis will explore this assumption.

Another important aspects regarding small vessel DP is the physical size of the vessel. Space, weight and economical issues limits the number of actuators that can be fitted on a small vessel. Because of this, it is hard to achieve independent movement in surge, sway and yaw, thus making the vessel under actuated. This

makes the control scheme hard, if not impossible, to solve for a vessel subject to environmental disturbances. The DP control problem has to be redefined. By disregarding the heading, some DP functionality can be achieved only by utilizing a underactuated surge and yaw propulsion system. This will be addressed later.

Other interesting aspects could be ways of improving fuel consumption or other intelligent systems that reduces the environmental forces acting on the vessel.

1.4 Previous Work

Filtering and state estimation are important features of a conventional DP system. The measured signal is often noisy and in worst case faulty. In addition, even though most GPS systems today provide velocity estimates, common practice is not to use these estimates in the DP system, as these velocities are computed by the GPS from the position measurements. Hence the state estimator in the DP system should be able to calculate the velocities from the measured heading and position. As mentioned, these measurements might be corrupted by noise due to wind, waves and ocean currents, as well as noise from the the sensors. In conventional DP systems designed for large vessels, only the slowly-varying disturbances should be counteracted by the thruster. To avoid oscillatory motion, such as 1st-order wave-induced disturbances, to enter the feedback loop a technique called wave filtering is used. When applying wave filtering to the measured signals, they are separated into a low-frequency (LF) motion and a wave-frequency (WF) motion. The reason to filter out these WF motions, is to reduce the wear and tear of the actuators, which will occur due to rapid changes in the control signal.

Dynamic positioning has not been widely applied on small vessels. Only in the recent year few attempts have been made. This is partially due to the lack of technology, but also economical, environmental and risk issues. For conventional DP systems, there have been written many papers on state estimation and a few about wave filtering, but very few, if any, has addressed this problem for a small vessel such as the USV.

- In Balchen et al. (1980) the Kalman Filter was introduced as state estimator for a DP system. Simulation results and actual recordings indicated excellent performance.
- In Fossen and Strand (1999) a nonlinear passive observer with wave filtering capabilities was developed and tested on a multipurpose supply vessel with excellent results. The advantage of this observer was the easier tuning (compared to a Kalman Filter), and that the equations of motions did not have to be linearized.

- In Lindegaard (2003) a nonlinear model based observer with wave filtering was proposed. It was based on the observer developed in Fossen and Strand (1999), but extended with the option to utilize both velocity and acceleration measurements in addition to the position and heading measurements. The observer was tested with Cybership II and gave good results.
- In Kjerstad (2010) a DP control system was developed and tested for the Viknes 830. Due to an under actuated vessel, the DP problem had to be redefined. A WOHC and a WOPC scheme was proposed. Both schemes performed satisfactory.

1.5 Scope

This thesis will build upon the work done in Kjerstad (2010) by trying to improve the DP system performance by implementing a state estimator. Energy consumption, convergence time and station keeping abilities are factors that are important and that could be improved. Especially, this thesis will explore to what extent wave filtering should be used in state estimation for small vessels. Two observers will be proposed, one model based observer that have the option of utilizing both velocity and acceleration measurements in addition to position and heading measurements, the other observer utilizes the measured acceleration as input to generate state estimates. Wave filtering will be applied in both cases in order to explore the benefits and drawbacks by using wave filter in the state estimation. The observers will be tested in the Viknes 830 simulator developed in Kjerstad (2010), and the goal is to test them on the real Viknes 830 owned by Maritime Robotics.

The observers will be compared against each other and against the performance without utilizing any of them. The factors that are important are:

- Actuator usage and thereby fuel and energy consumption. For a DP system i general, and especially for a unmanned vehicle, it is important to operate as fuel efficient as possible. The USV should be able to operate over long periods of time without the need for refueling.
- Station keeping ability. How well does the vessel maintain the desired position under different weather conditions. How well the USV maintains the desired position while being affected by wind, waves and current is an important feature of the DP system.
- The time it takes for the vessel to find the desired position. It is interesting to find out how long it takes for the USV to obtain the desired position from its initial position.

The following chapters are organized as follows:

- **Chapter 2** presents the vessel considered in this thesis, the Viknes 830 along with all of its features.
- **Chapter 3** introduce the Viknes 830 simulator. Detailed mathematical models of the vessel itself, the environmental disturbances and the controller are presented.
- **Chapter 4** presents the two observers in question. The Mathematical models and observer tuning are described.
- **Chapter 5** deals with simulation results. A test plan and test scenarios are presented, along with simulation results and discussion.
- **Chapter 6** is about the live experiments at sea with the Viknes 830. Results and discussion.
- **Chapter 7** concludes this thesis, and suggests future work and development

Chapter 2

Viknes 830

2.1 Introduction

Figure 2.1: The Viknes 830 at sea.

Figure 2.1 displays the Viknes 830 which is the vessel considered in this thesis. The Viknes 830 is a versatile leisure boat suited for most people. It is built to cope with typical Nordic conditions, and is manufactured by Viknes Båt og Service AS in Kleppestø, Norway under the slogan "Built for the North Sea". The main thruster is a conventional pitch propeller fixed to a shaft driven by an inboard engine. A traditional rudder in combination with an electrical tunnel thruster are the means of maneuvering. The Viknes 830 in question is owned by Maritime Robotics, a small Trondheim based research company. The vessel has been fitted with an

on-board computer (OBC) and additional sensors. This enables the Viknes 830 to operate as a versatile USV development platform, which makes room for the developer to participate in full scale experiments from inside the vessel. One of the latest additions to the USV was developed and tested in Kjerstad (2010), and is a small vessel DP system. The DP controller was implemented in Matlab Simulink and interfaced to the OBC through UDP packages.

2.2 Hull

The Viknes 830 has a semi-planing fiberglass hull and weights approximately 3.300 kg with standard equipment and fully bunkered. With the additional equipment installed by Maritime Robotics a slight increase in weight is assumed. Because the Viknes has a keel, the directional stability and the roll damping of the Viknes 830 is better compared to similar vessels without keel. Because the Viknes has most of its area above the water line, it is very susceptible to wind forces, which in turn can cause drift. Figure 2.2 displays the longitudinal dimensions of the Viknes.

Figure 2.2: The lateral dimensions of the Viknes.

2.3 Actuators

2.3.1 Engine and Gear

The Viknes 830 is fitted with a 135.6 kW Yanmar 4LHA-DTP diesel engine which is connected to a 1:2.03 ratio gear equipped with trolling capability. The trolling function enables the propeller shaft to rotate with a controlled slip relative to the fixed gear ratio, and is normally only available at low RPM. This is achieved with

a viscous layer of oil between two physically separated rotating discs. In trolling mode, the propeller RPM is controlled by adjusting the gap between the two discs.

2.3.2 Propeller

Figure 2.3 shows the Sleipner S-8 skew-back propeller. This is the propeller fitted to the Viknes 830. Skew-back propellers have asymmetrical propeller blade contours which, if you look from fore to aft, are swept backwards. This property creates less vibrations, higher top speed and lower fuel consumption, and is usual for medium to high speed propellers.

2.3.3 Rudder

As figure 2.2 shows, a conventional balanced rudder is installed directly behind the propeller. The area of the propeller is 0.15 m^2 and provides good maneuvering capabilities even at low speeds. A servo controls the rudder, enabling a rudder angle of $\pm 27°$.

Figure 2.3: The Sleipner S-8 skew-back propeller.

2.3.4 Tunnel Thruster

The Tunnel thruster is delivered by Sleipner AS. In Kjerstad (2010) it is found to be a fixed transverse directional on-off thruster, producing approximately 670 N of thrust when enabled. It has a maximum operation time of 2 minutes and 40 seconds in each sequence, and for long time usage the thruster should not run for more than 8% of the time. The thruster is mounted in a tunnel pipe just below the waterline in the bow, as can be seen in figure 2.2.

2.4 Custom Equipment and Interface

To be able to operate as an USV, the Viknes have been fitted with an extended equipment package. The OBC is the center of the system and it inputs position, yaw angle, velocity and yaw-rate from a Furuno SC-50 GPS compass and outputs commands through a digital to analog converter to the electromechanical devices electronically manipulating throttle, rudder and tunnel thruster. In addition, a Microstrain 3DM-GXI inertial measurement unit (IMU), which outputs linear acceleration, has been added to the system. The OBC runs an industrial control platform on top of a Linux operating system. The communication between the OBC and an external computer running the control system that calculates set-points to manipulate the outputs of the OBC happens through UDP data packages. For testing and development a laptop can be used to run the control system, but complete functioning systems should be implemented directly in the OBC. In this thesis the interface considered consists of a $\pm 0 - 100\%$ throttle wire setting, a -15 to 15 degree rudder setting and a -1, 0 or +1 tunnel thruster setting, where the thrust direction is determined by the sign -/+. The control system in this thesis is implemented in a Matlab Simulink environment which reads and sends commands to and from the vessel via UDP packages. Data sheets for the Furuno GPS antenna and the Microstrain IMU can be found in appendix A and B respectively

Figure 2.4: The Furuno SC-50 GPS compass.

2.5 DP System

The Viknes USV is not fitted with any permanent DP system. To get DP functionality, a laptop running the DP system in Simulink has to be connected to the OBC. This way, the DP controller can get sensor signals and keep the USV at the desired position. Since the Viknes 830 is fitted with a tunnel thruster, a rudder and a conventional propeller the vessel becomes underactuated as none of the actuators allow for independent sway motion. Due to this actuator configuration, a WOPC scheme was derived in Kjerstad (2010). The next chapter will present this scheme in more detail.

Chapter 3

Dynamic Positioning Simulator

3.1 Introduction

Before doing full scale experiments with a real vessel it is important to test the systems developed, in a simulator. By doing this, the developer will be able to discover bugs and bad design before implementing the system on a real vessel. Simulations also enables the developer to test various and unlikely scenarios, where the system performance can be tested to the extreme. In addition, testing and simulation have proved to make the development process less costly and more safe for the parties involved. In Kjerstad (2010), a DP control system was developed along with a mathematical model of the Viknes 830. The Viknes 830, the environmental disturbances and a DP controller was developed and implemented in Simulink. Many of the functions and Simulink blocks are adapted from Marine Systems Simulator (MSS) toolbox for Matlab and Simulink, developed by Marine Control. This thesis will continue to work with this simulator by adding an observer and by testing techniques to improve performance of the station keeping capabilities.

3.2 Reference Frames

To ease the analysis of vessel movement in 6 DOFs it is convenient to define some coordinate frames to use in the analysis. The necessary coordinate frames are presented in this section.

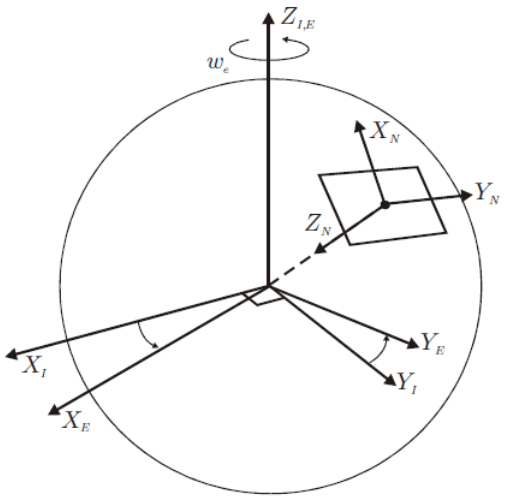

Figure 3.1: ECI, ECEF and NED reference frames.

ECI frame

This reference frame is called the Earth centered inertial (ECI). The origin of this frame is located in the origin of the Earth and does not follow the rotation of the planet. Because the Earth orbits the Sun the frame is not truly inertial, but for most applications the error is so small that it can be neglected. Newton's laws of motion apply in this frame.

ECEF frame

This is the Earth centered Earth fixed (ECEF) reference frame. It's origin is also located in the center of the Earth, and this frame rotates along with the planet. For marine crafts moving with low speed, the rotation of this frame can be neglected, and the ECEF frame can be considered inertial.

NED frame

The North-East-Down (NED) coordinate frame is defined as the tangent plane on the Earth's surface, fixed to the movement of the craft. With the x-axis (N) pointing towards true north, the y-axis (E) pointing east and the z-axis (D) pointing down, perpendicular to the tangent plane, this is the frame we refer to in everyday life. Because DP operations have little variations in longitude and latitude, it is convenient to use the NED frame for navigation. The NED frame is assumed to be inertial, hence Newton's laws of motion apply. The ECI, ECEF and NED frames are shown in figure 3.1 .

Body frame

The body frame is a vessel-fixed reference frame. It moves and rotates with the vessel. The origin is usually chosen to coincide with a point mid ship, and the

principal axes with axes of inertia. The body frame is used to relate the vessels position and orientation to an inertial frame. For a more comprehensive description of the different reference frames and their mathematical relations, see Kjerstad (2010).

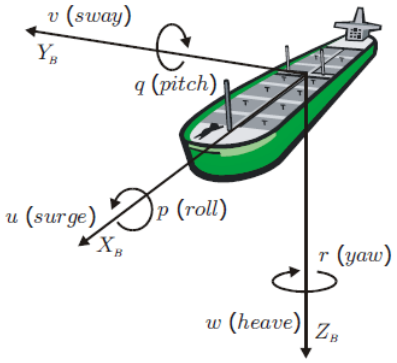

Figure 3.2: Illustration of the body-fixed frame and movements in different DOFs.

3.3 Viknes 830 6 DOF model

To be able to represent the Viknes 830 in a simulator, some vessel data needs to be calculated. This can be done in a hydrodynamical software, such as Veres ShipX. From Fossen (2011), a unified 6 DOF sea keeping and maneuvering model is described by

$$\dot{\boldsymbol{\eta}} = \mathbf{J}(\boldsymbol{\eta})\boldsymbol{\nu} \quad (3.3.1)$$

$$\mathbf{M}\dot{\boldsymbol{\nu}} + \mathbf{C}_{RB}(\boldsymbol{\nu})\boldsymbol{\nu} + \mathbf{C}_A(\boldsymbol{\nu}_r)\boldsymbol{\nu}_r + \mathbf{D}(\boldsymbol{\nu}_r)\boldsymbol{\nu}_r + \boldsymbol{\mu} + \mathbf{G}\boldsymbol{\eta} = \boldsymbol{\tau}_{\mathbf{env}} + \boldsymbol{\tau} \quad (3.3.2)$$

here, the vectors $\boldsymbol{\eta} = [x, y, z, \phi, \theta, \psi]^T$ and $\boldsymbol{\nu} = [u, v, w, p, q, r]^T$ are the position, orientation and velocity of the vessel given in in the NED and body frames respectively. Table 3.1 shows the relationship between the two vectors.

DOF		Forces and moments	Linear and angular velocities	Position and Euler angles
1	Motion in x-direction (surge)	X	u	x
2	Motion in y-direction (sway)	Y	v	y
3	Motion in z-direction (heave)	Z	w	z
4	Rotation about the x-axis (roll)	K	p	ϕ
5	Rotation about the y-axis (pitch)	M	q	θ
6	Rotation about the z-axis (yaw)	N	r	ψ

Table 3.1: SNAME (1950) notation for marine vessels

3.3.1 Inertia

The mass of the vessel, represented by the **M**-matrix, consists of two separate terms

$$\mathbf{M} = \mathbf{M}_{\text{RB}} + \mathbf{M}_A \tag{3.3.3}$$

The $\mathbf{M}_{RB}$ matrix is the physical rigid-body mass of the vessel, while the M_A-matrix is called the added mass matrix. The added mass is a hydrodynamical phenomenon that happens when an object moves through water. When a vessel accelerates or decelerates, it imposes an acceleration or a deceleration on the surrounding fluid. This fluid movement will, from the vessels point of view, be interpreted as additional mass. In general, this hydrodynamical added mass matrix is dependent on the frequency of motion due to water surface effects, but in Fossen (2011) it is stated that this matrix can be approximated to a constant frequency, assuming that the surge motion is decoupled and that the vessel is port-starboard symmetric. The total mass matrix can therefore be composed as

$$\mathbf{M} = \begin{bmatrix} m - X_{\dot{u}} & 0 & 0 & 0 & -mz_g & my_g \\ 0 & m - Y_{\dot{v}} & 0 & -mz_g - Y_{\dot{p}} & 0 & mx_g - Y_{\dot{r}} \\ 0 & 0 & m - Z_{\dot{w}} & my_g & -mx_g - Z_{\dot{q}} & 0 \\ 0 & -mz_g - K_{\dot{v}} & my_g & I_x - K_{\dot{p}} & -I_{xy} & -I_{xz} - K_{\dot{r}} \\ mz_g & 0 & -mx_g - M_{\dot{w}} & -I_{yx} & I_y - K_{\dot{q}} & -I_{yz} \\ -my_g & mx_g - N_{\dot{v}} & 0 & -I_{zx} - N_{\dot{p}} & -I_{zy} & I_z - N_{\dot{r}} \end{bmatrix} \tag{3.3.4}$$

3.3.2 Coriolis and Centripetal Forces

Coriolis and centripetal forces

The term $\mathbf{C}_{RB}(\boldsymbol{\nu})$ and $\mathbf{C}_{A}(\boldsymbol{\nu})$ represent the Coriolis and centripetal forces acting on the vessel. These effects appear due to the dynamics of the non-inertial body frame. Both terms are nonlinear, but according to Fossen (2011) both terms can be linearized around the forward velocity of the vessel. The stated result is

$$\mathbf{C}^{*}_{RB} = U\mathbf{M}_{RB}\mathbf{L} \tag{3.3.5}$$

$$\mathbf{C}^{*}_{A} = U\mathbf{M}_{A}\mathbf{L} \tag{3.3.6}$$

where U is the relative water speed, and $\mathbf{L}$ is a selection matrix, defined as.

$$\mathbf{L} = \begin{bmatrix} 0 & 0 & 0 & 0 & 0 & 0 \\ 0 & 0 & 0 & 0 & 0 & 1 \\ 0 & 0 & 0 & 0 & -1 & 0 \\ 0 & 0 & 0 & 0 & 0 & 0 \\ 0 & 0 & 0 & 0 & 0 & 0 \\ 0 & 0 & 0 & 0 & 0 & 0 \end{bmatrix} \tag{3.3.7}$$

3.3.3 Damping Forces

All marine vessels will experience hydrodynamical damping due to the displacement of water. Potential damping, skin friction, wave drift forces, lifting forces and damping due to vortex shedding are all contributors to this. The damping term $\mathbf{D}(\boldsymbol{\nu}_r)$ of equation 3.3.2, can be separated into a linear and a nonlinear term

$$\mathbf{D}(\boldsymbol{\nu}_r) = \mathbf{D}_L + \mathbf{D}(\boldsymbol{\nu}_r) \tag{3.3.8}$$

Here, $\boldsymbol{\nu}_r$ is the velocity relative to the water, which means that the vessel can have velocity above the water surface without being affected by damping forces. The linear term can be represented as linear matrix because of symmetry around the xz-plane:

$$\mathbf{D}_L = -\begin{bmatrix} X_u & 0 & 0 & 0 & 0 & 0 \\ 0 & Y_v & 0 & Y_p & 0 & Y_r \\ 0 & 0 & Z_w & 0 & Z_q & 0 \\ 0 & K_v & 0 & K_p & 0 & K_r \\ 0 & 0 & M_w & 0 & M_q & 0 \\ 0 & N_v & 0 & N_p & 0 & N_r \end{bmatrix} \tag{3.3.9}$$

The nonlinear contribution can be separated into two independent phenomenas, nonlinear surge damping and cross-flow drag.

The nonlinear surge damping is a prevailing surge damping when the velocity reaches a certain level. The surge damping can be modeled as

$$X = X_{|u|u} |u_r| u_r \tag{3.3.10}$$

where

$$X_{|u|u} = \frac{1}{2}\rho A_x C_X \tag{3.3.11}$$

and C_X is the surge damping coefficient. The nonlinear damping term is intuitively a quadratic term, but is only applicable as long as the vessel does not lift itself out of the water due to increasing velocity. If this should happen, the equation is no longer valid.

Cross-flow drag is the damping in sway and yaw. It can be computed by using the principles given in **?**, and the equations for sway and yaw respectively become

$$Y = -\frac{1}{2}\rho \int_{\frac{-L_{pp}}{2}}^{\frac{L_{pp}}{2}} T(x) C_d^{2D}(x) |v_r + xr| (v_r + xr) dx \tag{3.3.12}$$

$$N = -\frac{1}{2}\rho \int_{\frac{-L_{pp}}{2}}^{\frac{L_{pp}}{2}} T(x) C_d^{2D}(x) |v_r + xr| (v_r + xr) dx \tag{3.3.13}$$

C_d^{2D} is the 2D drag coefficient found in Hoerner's curve. $T(x)$ is the vessel draft and v_r is the relative sway velocity.

3.3.4 Restoring Forces

Heave, roll and pitch movement of the vessel will always be counteracted by something called the restoring forces. These restoring forces are usually called the meta centric stability of the vessel. Figure 3.3 illustrates the concept. It can be regarded as a mass-damper-spring system trying to push the vessel to its equilibrium position in heave, roll and pitch. A movement in roll will displace the center of buoyancy (CB), whereas the center of gravity (CG) will always be fixed at the

same point. This creates the transverse righting arm (GZ), which in this case tries to restore the roll to equilibrium.

The GMt length is an important measure of stability. This is the transversely meta centric height. A large GMt will act as a stiff spring, highly stabilizing, but uncomfortable for passengers.

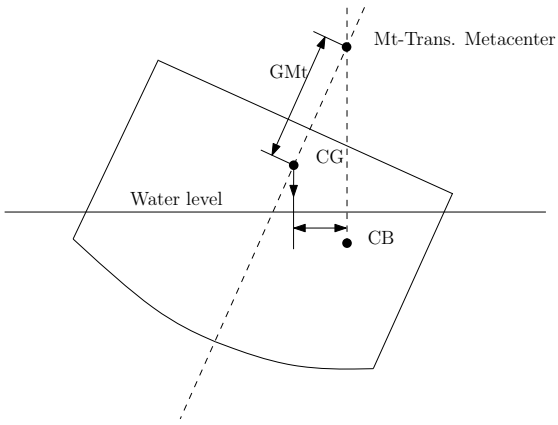

Figure 3.3: Restoring forces acting on a rolling vessel.

In Fossen (2011) the restoring forces are approximated as

$$\mathbf{G} = \begin{bmatrix} 0 & 0 & 0 & 0 & 0 & 0 \\ 0 & 0 & 0 & 0 & 0 & 0 \\ 0 & 0 & -Z_z & 0 & -Z_\theta & 0 \\ 0 & 0 & 0 & -K_\phi & 0 & 0 \\ 0 & 0 & -M_z & 0 & -M_\phi & 0 \\ 0 & 0 & 0 & 0 & 0 & 0 \end{bmatrix} \tag{3.3.14}$$

due to linearization and symmetry in the $xy-$plane.

3.3.5 Fluid Memory Effects

A moving vessel will generate waves, which in turn affects the vessel. This phenomenon is called fluid memory effects and is represented by the $\boldsymbol{\mu}$ term in 3.3.2, and has the following dynamics

$$\dot{\mathbf{x}} = \mathbf{A}_r + \mathbf{B}_r \delta\boldsymbol{\nu} \tag{3.3.15}$$

$$\boldsymbol{\mu} = \mathbf{C}_r \mathbf{x} \tag{3.3.16}$$

3.3.6 Driving Forces

The remaining terms in equation 3.3.2 are driving forces. $\boldsymbol{\tau}_{env} = \boldsymbol{\tau}_{wind} + \boldsymbol{\tau}_{waves}$ and are environmental forces, and $\boldsymbol{\tau}$ are the control forces from the controller.

3.3.7 Actuator Models

Main Propulsion

As mentioned in Chapter 2, the vessel main propulsion consists of a diesel engine with a trolling gear connected to the propeller via a shaft. The interface is a $\pm 100\%$ throttle value. It is assumed that each throttle step corresponds to a given rpm, which simplifies the engine to a low pass filter of the desired throttle value. The engine model becomes

$$\dot{\omega} = k_{\omega} \left(-\omega + \omega_d \left(\vartheta \right) \right) \tag{3.3.17}$$

Here, ω is the actual rpm and $\omega_d(\vartheta)$is the desired rpm which is dependent on the throttle input to the interface ϑ. In Kjerstad (2010) it is mentioned that this engine model is not very accurate due to several reasons. First, the real engine cannot achieve rpms lower than a certain threshold since it would stop. The trolling gear enables propeller shaft rpm lower than the crankshaft of the vessel, but it is assumed to have different dynamics. It is also pointed out that despite different dynamics, physical investigations have revealed that the whole system can be regarded as a low pass filter of the desired input. The propeller shaft rpm is geared down compared to the crankshaft with a given gear ratio

$$\omega_p = k_{gr} \omega \tag{3.3.18}$$

where ω_p is the propeller shaft rpm and k_{gr} is the gear ratio. In Fossen (2011), the generated propeller thrust is suggested to be

$$X_p = T_{n|n|} n \left| n \right| - T_{|n|u_a} \left| n \right| u_a \tag{3.3.19}$$

where the parameters $T_{n|n|}$, $T_{|n|u_a}$ and u_a are given by

$$T_{n|n|} = \rho D^4 \alpha_2 \tag{3.3.20}$$

$$T_{|n|u_a} = \rho D^3 \alpha_1 \tag{3.3.21}$$

$$u_a = (1 - w) u \tag{3.3.22}$$

α_1 and α_2 are constants, D is the propeller diameter, ρ is the density of water and w is the wake friction number generated by the water movement along the vessel. The propeller shaft rpm, ω_p is converted to $\left[\frac{1}{s}\right]$ by

$$n = \frac{\omega}{60} \tag{3.3.23}$$

There might be small deviations from the model characteristics to the real propeller characteristics. The real propeller might create a small pitch angle, but since we assume low speed, this pitch contribution would be minimal and can therefore be omitted. The vessel might also experience a small contribution to the yaw rate due to the rotation of the propeller shaft, but this effect is also disregarded.

Rudder

The rudder system consists of a rudder servo, some mechanics and the rudder itself. The OBC inputs a desired rudder angle to the servo through the interface. The servo can be regarded as a low pass filtering of the desired angle δ_d

$$\dot{\delta} = k_\delta(-\delta + \delta_d) \tag{3.3.24}$$

here, δ is the actual rudder angle. k_δ is an system time constant to fit the real world system. The rudder generates forces in 4 DOFs

$$X_r = \frac{1}{2}v_r^2\rho A\left(\frac{\left(\frac{\delta C_L}{\delta\alpha_e}\delta\right)^2}{0.9\pi a_r} + C_{D0}\right) \tag{3.3.25}$$

$$Y_r = \frac{1}{2}v_r^2\rho\frac{\delta C_L}{\delta\alpha_e}\delta \tag{3.3.26}$$

$$K_r = -\left(VCG - \frac{1}{2}s_p\right)\frac{1}{2}v_r^2\rho A\frac{\delta C_L}{\delta\alpha_e}\delta \tag{3.3.27}$$

$$N_r = -LCG\frac{1}{2}v_r^2\rho A\frac{\delta Cl}{\delta\alpha_e}\delta \tag{3.3.28}$$

the parameters in equations 3.3.25 - 3.3.28 are dependent on the size and shape of the rudder. Table 3.2 explains the different parameters.

δ	Rudder angle
$\frac{\delta C_L}{\delta \alpha_e}$	Rudder lift coefficient
ρ	Water density
v_r	Relative water speed
A	Rudder area
a_r	Aspect ratio
D_{D0}	Drag coefficient at zero angle of attack
s_p	Rudder span
VCG	Vertical distance to center of gravity
LCG	Lateral distance to center of gravity

Table 3.2: Rudder parameters

3.3.8 Tunnel Thruster

The tunnel thruster is an electric motor combined with a small propeller. As mentioned earlier, this is an on-off thruster which is governed by a directional control signal given by

$$C_{TT} = \begin{cases} 1 & Starboard\, rotation \\ 0 & Thruster\, off \\ -1 & Port\, rotation \end{cases} \tag{3.3.29}$$

The actuator dynamics is modeled as a first order process with an adjusted time constant

$$\dot{\alpha} = k_\alpha(-\alpha + \alpha_d(C_{TT})) \tag{3.3.30}$$

Based on C_{TT}, α_d can be defined as

$$\alpha_d(C_{TT}) = k_{kg} C_{TT} \tag{3.3.31}$$

where k_{kg} is a constant thrust in kg described in the manufacturer's data-sheet. The produced yaw moment of the tunnel thruster can now be written

$$N_{TT} = 9.81 LCG\alpha \tag{3.3.32}$$

Total Control Forces

To summarize, the total control forces and moments are as follows:

$$X_c = X_p + X_r \tag{3.3.33}$$
$$Y_c = Y_r \tag{3.3.34}$$
$$Z_c = 0 \tag{3.3.35}$$
$$K_c = K_r \tag{3.3.36}$$
$$M_c = 0 \tag{3.3.37}$$
$$N_c = N_{TT} + N_r \tag{3.3.38}$$

3.4 Environmental Disturbances

To simulate a vessels behavior at sea, the naturally occurring forces acting on the vessel needs to be modeled. The main objective of a DP system is to keep the vessel at a given position independent of the environmental disturbances, it would be of little purpose to simulate such a system without the environmental forces acting on the vessel. The forces to consider are sea current, waves and wind. They can be modeled as independent phenomenas, or as one single disturbance since the rigid body of the vessel will experience one force, a sum of the environmental disturbance vectors.

3.4.1 Sea Current

Currents are caused by several forces such as gravitational and temperature difference based forces, caused mainly by the Moon and the Sun. These forces act on large areas of water and causes the equilibrium of the oceans to shift, generating massive movements of water. When considering currents in a DP system, it can be seen as a constant and uniform movement of water surrounding the vessel. By augmenting equation 3.3.1, current can be introduced in the vessel model

$$\dot{\boldsymbol{\eta}} = \mathbf{R}(\psi)\,\boldsymbol{\nu} + \boldsymbol{v}_c \tag{3.4.1}$$

The current velocities have predefined direction and magnitude

$$\boldsymbol{v}_c = [V_c cos(\beta_c)\ \ V_c sin(\beta_c)] \tag{3.4.2}$$

where V_c is the magnitude and β_c is the direction in the NED frame. It is assumed that the vessel heading is not influenced.

3.4.2 Waves

Waves are generated by wind sweeping the ocean surface, and is a complex phenomena. Ocean waves are considered to be irregular, which means that they are random in both time and space. It is common to consider local sea level as a realization of a stationary stochastic process. A wave spectrum can be used to describe the energy distribution in the frequency domain of the ocean surface. The spectrum will be dependent on the location of operation because of variations in the energy distribution.

The two most important measures of describing waves are the frequency of the waves, and the significant wave height. The significant wave height is defined as the mean wave height of the one-third largest waves in the sea state. For instance, if the sea state has a significant wave height of 2 [m], the common waves are smaller, however larger waves will also occurs. The wave frequency also plays an important role when characterizing waves, and waves can be divided into first-order and second order wave excitation forces depending on the frequency. The first-order wave forces are the high frequency wave motion, also known as the zero-mean oscillatory motion or the Wave Frequency (WF) motion. The second-order wave motion includes wave-drift loads and slowly varying wave loads. It is the slowly-varying disturbances the controller should counteract.

3.4.3 Wind

Wind is the movement of air above the Earth's surface. Similar to waves it will affect the vessel depending on the angle of attack. In addition, the shape of the vessel and the projected area towards the wind will be important. Wind is normally modeled as a mean wind with random fluctuations called gust. In practice this could be be implemented as a random walk process added to a constant term. The wind disturbance will act as a resultant force constantly trying to push the vessel away from the desired position. In Fossen (2011), the wind forces is described as

$$\boldsymbol{\tau}_{wind} = \frac{1}{2}\rho_a V_{rw}^2 \begin{bmatrix} C_X\left(\gamma_{\omega_{rw}}\right) A_{Fw} \\ C_Y\left(\gamma_{\omega_{rw}}\right) A_{Lw} \\ C_Z\left(\gamma_{\omega_{rw}}\right) A_{Fw} \\ C_K\left(\gamma_{\omega_{rw}}\right) A_{Lw} H_{Lw} \\ C_M\left(\gamma_{\omega_{rw}}\right) A_{Fw} H_{Fw} \\ C_N\left(\gamma_{\omega_{rw}}\right) \rho_a V_r^2 A_{Lw} L_{oa} \end{bmatrix} \tag{3.4.3}$$

where the relative wind speed and the angle of attack is given by

$$V_{rw} = \sqrt{u_{rw}^2 + v_{rw}^2} \tag{3.4.4}$$

$$\gamma_{rw} = -atan2(v_{rw}, u_{rw}) \tag{3.4.5}$$

and the parameters described in table 3.3 can be found through experiments or estimation.

γ_ω	Relative wind angle
C_i	Wind coefficients
A_{Fw}	Frontal projected area
A_{Lw}	Lateral projected area
H_{Fw}	Frontal centroid above the water line
H_{Lw}	Lateral centroid above the water line
L_{oa}	Vessel overall length

Table 3.3: Wind forces and moments parameters

To describe the environmental conditions acting on a vessel at sea, several alternatives exist. The most widely accepted system is the Beaufort wind force scale. The scale characterize the sea conditions depending on wind and wave magnitude. The original Beafort scale is not meant to provide a good measure close to shore, and the wind speeds are therefore measured 10 [m] above the sea level. In table 3.4, a modified scale is displayed. This scale is modified to give a realistic characterization at 1 [m] above sea level.

Beaufort nbr	Description	Wind speed	Wave height	Sea conditions
0	Calm	< 0.1 m/s	0 m	Calm (glassy).
1	Light air	0.1-0.6 m/s	0-0.2 m	Calm (rippled).
2	Light breeze	0.6-1.3 m/s	0.2-0.5 m	Smooth (wavelets).
3	Gentle breeze	1.3-2.1 m/s	0.5-1 m	Slight.
7	Moderate breeze	2.1-3.1 m/s	1-2 m	Slight-Moderate.
5	Fresh breeze	3.1-4.3 m/s	2-3 m	Moderate.
6	Strong breeze	4.3-5.5 m/s	3-4 m	Rough.
7	Near gale	5.5-6.8 m/s	4-5.5 m	Rough-Very rough
8	Gale	6.8-8.2 m/s	5.5-7.5 m	Very rough-High
9	Severe gale	8.2-9.7 m/s	7-10 m	High
10	Storm	9.7-11.3 m/s	9-12.5 m	Very High
11	Violent storm	11.3-13.0 m/s	11.5-16 m	Very High
12	Hurricane	> 13.0 m/s	> 14 m	Phenomenal

Table 3.4: The Beaufort wind force scale. Wind measured at 1 m.

3.5 Dynamic Positioning Controller

3.5.1 Control Scheme

In order for the Viknes 830 to achieve station keeping abilities with the current thruster configuration, a sway independent control scheme must be considered. As mentioned, ordinary DP schemes is not sway independent and is therefore unsuitable for the Viknes. Instead, the station keeping problem is redefined. Since the vessel considered has no means of controlling sway motion, the environmental forces acting on the vessel will be regarded as a force field. By utilizing this force field in addition to independent movement in surge and yaw, a scheme where the vessel keeps a distance and heading towards a given point can be created. The tunnel thruster and rudder controls the heading, and the propeller controls the distance. Now, station keeping is redefined to be the ability to hold a position on a circle around a given point. This is known as weather optimal heading control (WOHC). This scheme is analogous to a pendulum in a force field.

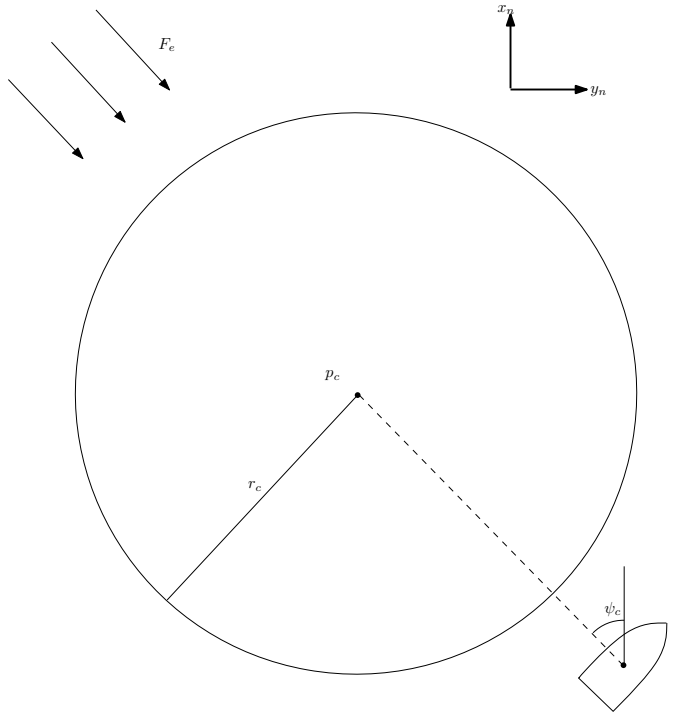

Figure 3.4: Illustration of the vessel as a virtual pendulum influenced by an environmental force field.

By moving the pendulum suspension point to get a coincidence between the desired position and the vessel, weather optimal positioning control (WOPC) is achieved.

This approach has both pros and cons. The pros is of course that an underactuated vessel will be able to do station keeping. The cons on the other hand is the convergence time dependency from environmental forces and the inability of heading predetermination. If the environmental forces are strong, the convergence is fast, whereas weak forces yields slow convergence. In this scheme, the vessel heading is always opposite of the force field direction.

3.5.2 Weather Optimal Heading Control

In a WOHC scheme, the vessel will position itself with a heading in the opposite direction of the environmental force field, and a distance from the suspension point of the pendulum. This distance can be regarded as the pendulum radius, and suspension point is denoted $\boldsymbol{p_c} \triangleq [x_c, y_c]^T$. To derive the WOHC, the deviations from the suspension point $\boldsymbol{p_c}$ is defined as follows:

$$\tilde{x} \triangleq x_c - x \tag{3.5.1}$$
$$\tilde{y} \triangleq y_c - y \tag{3.5.2}$$

The pendulum scheme has one stable and one unstable equilibrium point. This comes from the fact that two positions on a pendulum arc align with the resultant force. These two positions corresponds to a normal pendulum and an inverted pendulum. In the real world it is impossible for the vessel to end up in the unstable inverted pendulum position because small disturbances will push it away from this position. It will instead converge to the stable equilibrium where the heading is 180 $[deg]$ opposite of the resultant force. To create a virtual pendulum line, a surge and an yaw controller is used.

Surge Control

The surge controller aims to position the body-fixed deviation to become the pendulum arc radius r_c. The body-fixed deviations towards the suspension point can be described by

$$\boldsymbol{e_b} = R^T(\psi) \begin{bmatrix} (\sqrt{\tilde{x}^2 + \tilde{y}^2} - r_c)cos\psi_c \\ (\sqrt{\tilde{x}^2 + \tilde{y}^2} - r_c)sin\psi_c \\ 0 \end{bmatrix} \tag{3.5.3}$$

such that the body-fixed surge deviation becomes

$$\begin{aligned} e_{b,surge} &= (\sqrt{\tilde{x}^2+\tilde{y}^2}-r_c)cos\psi_c cos\psi \\ &- (\sqrt{\tilde{x}^2+\tilde{y}^2}-r_c)sin\psi_c sin\psi \end{aligned} \tag{3.5.4}$$

here, ψ_c is defined to be

$$\psi_c \triangleq atan2(\tilde{x},\tilde{y}) \tag{3.5.5}$$

which is the heading towards $\boldsymbol{p_c}$ defined in NED. The surge control law τ_{surge} becomes

$$\tau_{surge} = K_{d_s}(\tilde{u}) + K_{i_s}\int \kappa_i e_{b,surge} d\tau \tag{3.5.6}$$

For a more thorough explanation and derivation of the surge controller see Kjerstad (2010).

Yaw Control

The purpose of the yaw controller is to direct the heading of the vessel towards the pendulum suspension point. The Viknes 830 has two different actuators that manage the heading. It is therefore necessary with two controllers and a switching algorithm to switch between them.

The switching between the controllers is a relay scheme, where the relative water speed u_p is the switching argument. Since the rudder is inefficient at low velocities, while the tunnel thruster is of little use at high, suggests that only one of the yaw actuators should be used at a time. By using a hysteresis scheme the vessel will never end up in a situation where both actuators are turned off due to small perturbations. It ensures that one controller always is enabled.

The rudder and the tunnel thruster controllers both have the same structure. The controller is using a scale independent angular velocity profile with the ψ deviation as input. The structure is as follows

$$\tau_\psi = K_{d_\psi}(\tilde{r}), \tag{3.5.7}$$

$$\tilde{r} \triangleq r_d - r \tag{3.5.8}$$

where

$$r_d = r_{max} tanh(\frac{\tilde{\psi}}{r_{max} \triangle r}), \tag{3.5.9}$$

$$\tilde{\psi} \triangleq \psi_c - \psi \tag{3.5.10}$$

here, the desired heading ψ_c is defined by 3.5.5. The controllers are only different in tuning of the angular velocity profile and the proportional gain. For the tunnel thruster, it is desirable to set $K_\psi = 1$ because this gives a more intuitive thrust allocation due to working with the actual yaw rate deviation.

Control Vector

To emulate the pendulum, the resulting control vector becomes

$$\boldsymbol{\tau} = \begin{bmatrix} K_{d_s}(u_d - u) + K_{i_s} \int_0^t \kappa_i e_{b,surge} d\tau \\ 0 \\ K_{d_\psi}(r_d - r) \end{bmatrix} \tag{3.5.11}$$

where K_{d_S}, K_{i_s} and K_{d_ψ} are gains of a PD controller. Since the sway forces are set to 0 the vessel becomes underactuated.

3.5.3 Weather Optimal Positioning Control

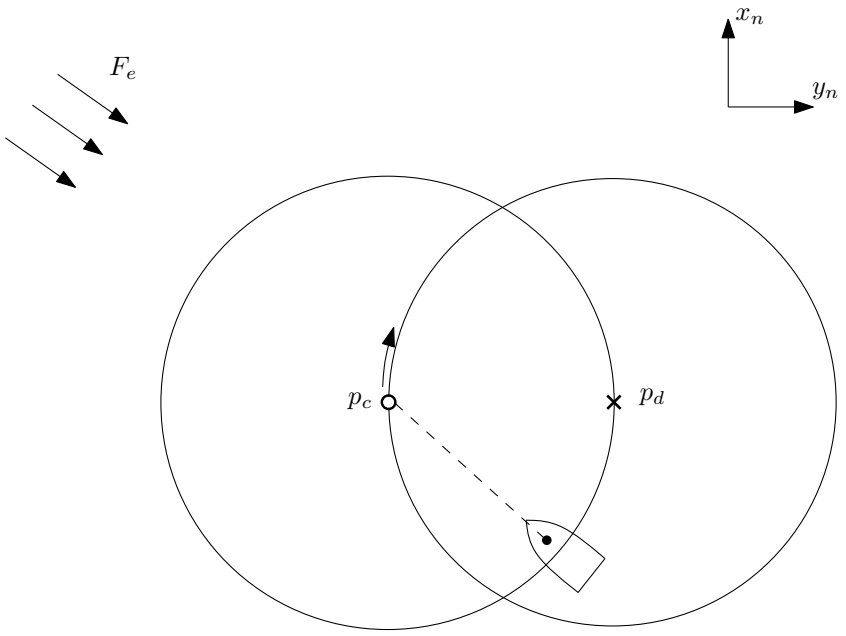

Figure 3.5: Illustration of WOPC. The suspension point p_c is moved such that the vessel may be positioned at p_d.

As mentioned earlier, a WOPC scheme can be achieved by moving controlling the pendulum suspension point p_c. Figure 3.5 demonstrates this this principle. The surge and yaw controller emulates a virtual pendulum, while another controller moves the suspension point p_c. By drawing circles around p_c and p_d with a radius r_c, it becomes evident that the suspension point p_c must lie on a circle arc of p_d for the vessel to converge to p_d. By modeling the movement of p_c as a first order system, a simple control law can be derived. The objective is to remove the angular deviation between the heading of the vessel, ψ, and the desired heading ψ_d. Vessel deviation from the suspension point is given by equations 3.5.1 and 3.5.2, and the deviation between p_d and p_c is defined as

$$\tilde{x}_{cd} = x_c - x_d \tag{3.5.12}$$
$$\tilde{y}_{cd} = y_c - y_d \tag{3.5.13}$$

The angle between p_d and p_c is defined as

$$\psi_d = atan2(\tilde{y}_{cd}, \tilde{x}_{cd}) \tag{3.5.14}$$

and the deviation to minimize is

$$\tilde{\psi}_{cd} = \psi_c - \psi_d \tag{3.5.15}$$

Now, ψ_d is modeled as a first order system

$$\dot{\psi}_d = k(\epsilon)\tilde{\psi}_{cd} \tag{3.5.16}$$

where $k(\epsilon)$ is a adaptive gain defined as

$$k(\epsilon) = \epsilon + \xi \tag{3.5.17}$$

where ξ is a constant to ensure a minimum of movement. The dynamics of ϵ is

$$\dot{\epsilon} = k_\epsilon(-\epsilon + \left|\dot{\psi}_c\right|) \tag{3.5.18}$$

The adaptive gain enables the system to move p_c with an angular velocity that is proportional to the strength of the environmental force field. A to low or a to high adaptive gain would degrade the convergence time and the performance of the positioning controller.

The position of the suspension point p_c can now be calculated from the following equations

$$x_c = r_c cos(\psi_d) + x_d \tag{3.5.19}$$
$$y_c = r_c sin(\psi_d) + y_d \tag{3.5.20}$$

The suspension point controller moves p_c, which is the set point of the virtual pendulum controller, and the pendulum analogy is complete. The WOHC scheme creates the virtual pendulum, trying to get the vessel to point towards p_c at a distance r_c. To achieve WOPC, a circle controller moves p_c around the desired position, making it possible for the vessel position to coincide with the desired position. It is also required that the bandwidth of the virtual pendulum WOHC is relatively higher than the suspension point controller.

3.5.4 Thrust Allocation

The set-points delivered from the controller has to be converted to inputs that can be used by the vessel. For instance, the force set-point delivered from the surge

controller has to be converted to a throttle set-point in order to work with the vessel. The delivered force X is converted to angular velocity through

$$\omega = \frac{X}{|X|}\sqrt{\frac{|X|}{\rho d^4 \alpha_2}} + ku_a \tag{3.5.21}$$

The tunnel thruster control delivers an angular velocity deviation that is converted to a control signal:

$$TT(r_d - r) = \begin{cases} 1 & if\,(r_d - r) > 0\,and\,\psi_d - \psi > \Phi \\ -1 & if\,(r_d - r) < 0\,and\,\psi_d - \psi < -\Phi \\ 0 & else \end{cases} \tag{3.5.22}$$

where Φ is the magnitude of a breaking zone defined in Kjerstad (2010). The rudder controller delivers a moment. This moment is converted to a rudder angle with the following formula

$$\delta = \frac{2N}{u_p^2 \rho A \frac{dC_L}{dA_e} LCG} \tag{3.5.23}$$

The parameters of equation 3.5.23 are given in table 3.5.

δ	Rudder angle
$\frac{\delta C_L}{\delta \alpha_e}$	Rudder lift coefficient
ρ	Water density
v_r	Relative water speed
A	Rudder area
a_r	Aspect ratio
D_{D0}	Drag coefficient at zero angle of attack
s_p	Rudder span
VCG	Vertical distance to center of gravity
LCG	Lateral distance to center of gravity

Table 3.5: Rudder parameters

Chapter 4

Observer Design

4.1 Introduction

A typical vessel has several sensors that measures the different states of the system. These measurements are often noisy and in worst case distorted due to disturbances. An observer should be able to filter all available measurements in order to provide on line estimates of both measured and unmeasured states. In conventional ship control the observer filters out the high frequency wave motion and leaves the low-frequency parts of the position, heading and velocity measurements. The stationary and slowly varying effects caused by wind and ocean currents are also kept in the measurements. The DP controller receives the estimates states, and based on these the thruster set points are calculated. Conventional DP observers have three main objectives:

- State estimation: The observer has to produce correct state estimates for the controller to be able to calculate propeller thrust forces and moments.
- Wave filtering: To avoid wear and tear on the thruster system, the observer should filter out high frequency oscillatory motion caused by first-order wave loads. Counteracting the zero mean behavior is pointless and would only lead to excessive thruster usage.
- Dead-reckoning: In the case of missing measurements either due to temporary sensor failure, or some other failure, the observer should be able to deliver satisfactory estimates for a period of time such that the vessel can maintain its DP capabilities. This is also a redundancy requirement posed by the classification societies.

The classical and most common solution to the DP state estimation problem is to use stochastic theory (Kalman filters) and filter out the 1st-order wave induced motion, see Balchen et al. (1980).

In this paper, a small vessel USV is considered, and this poses new requirements on the observer to be used. A small vessel is more vulnerable to the environmental disturbances, especially the disturbances caused by the ocean waves. While larger ships can cope better with high frequency wave motion, a smaller vessel like the USV, will be much more sensitive to this rapid motion. According to Lindegaard (2003), the vessel station keeping performance might be enhanced by utilizing the measured acceleration in the state estimation. In addition, the state estimates can be improved by using the measured velocity. It is therefore desirable to have an observer that has the option of using both measured acceleration, and measured velocity to improve the state estimates.

In this paper, two observers will be proposed. One simple observer using the measured acceleration as input to get estimates of the position and velocity, and one model based observer based on the observer developed in Lindegaard (2003). Both observers incorporate a wave filter that can be tuned according to the weather conditions at the location of operation. Both observers will be tested in different weather conditions, and will be evaluated according the criteria stated in chapter 1.

4.2 Wave Filtering

During DP operations, the vessel will experience external forces acting on it. Wind, currents and waves are all forces that tries to push the vessel away from the desired position, and the DP system has to counteract all these forces with the thrusters available. However, in conventional DP systems only the slowly varying disturbances are counteracted, whereas the oscillatory motion due to waves are kept out of the feedback loop. This is done in order to reduce the wear and tear of the different actuators and to reduce the fuel consumption. A technique called wave filtering separates the position and heading measurements into a low-frequency (LF) and a wave-frequency (WF) position and heading estimates, and thus it is possible to leave out the WF motion from the feedback loop. In Fossen and Strand (1999), wave filtering is defined as follows:

Definition 3 (Wave Filtering). *Wave Filtering can be defined as the reconstruction of the LF motion components* $\boldsymbol{\eta}$ *from the noisy measurement* $\boldsymbol{y} = \boldsymbol{\eta} + \boldsymbol{\eta}_w + \boldsymbol{v}$ *by the means of an observer. In addition to this, a noise-free estimate of the LF velocity* $\boldsymbol{\nu}$ *should be produced by* $\boldsymbol{y}$*. This is crucial in ship motion control systems since the oscillatory motion* $\boldsymbol{\eta}_w$ *due to 1st-order wave -induced disturbances will,*

if it enters the feedback loop, cause wear and tear of the actuators and increase the fuel consumption.

An important remark is that in general it is impossible to counteract the 1st-order wave induced motion of a ship when applying a reasonable propulsion and thruster system. Hence, feeding back the WF motion to the controller would not enhance the performance.

In general, a linear WF model of order p can be described by

$$\dot{\boldsymbol{x}}_w = \boldsymbol{A}_w \boldsymbol{x}_w + \boldsymbol{E}_w \boldsymbol{w}_w \tag{4.2.1}$$
$$\boldsymbol{y}_w = \boldsymbol{C}_w \boldsymbol{x}_w \tag{4.2.2}$$

where $\boldsymbol{x}_w \in \mathbb{R}^{3n_i}$, $\boldsymbol{w}_w \in \mathbb{R}^3$ and $\boldsymbol{A}_w$, $\boldsymbol{E}_w$ and $\boldsymbol{C}_w$ are constant matrices of appropriate dimensions. n_i is the number of available measurements. It is assumed that $\boldsymbol{w}_w$ are zero-mean Gaussian white noise. In this thesis, a fourth order model will be used. The reason for this is that the wave spectrum approximation will be better, and because the transfer functions between the excitation and positions, velocities as well as accelerations, will be strictly proper. A fourth order wave induced motion model can be described by two second order linear systems in cascade. The system matrices in each DOF become

$$\boldsymbol{A}_w = \begin{bmatrix} \boldsymbol{0} & \boldsymbol{I} \\ -\boldsymbol{\Omega} & -\boldsymbol{\Lambda} \end{bmatrix}, \boldsymbol{C}_w = \begin{bmatrix} \boldsymbol{0} & \boldsymbol{I} \end{bmatrix} \tag{4.2.3}$$

Here, each DOF is separated from the others by setting

$$\boldsymbol{\Omega} = diag(\omega_1^2, ..., \omega_{n_{y,i}}^2) \tag{4.2.4}$$
$$\Lambda = diag(2\zeta_1\omega_1, ..., 2\zeta_{n_y}\omega_{n_{y,i}}) \tag{4.2.5}$$

where $\omega_k > 0$ is the resonance frequency, $\zeta_k > 0$ is the relative damping factor which determines the width of the spectrum, and $n_{y,i}$ is the number of available measurements.

For a fourth order system, the transfer function from measurement to LF estimate is given by

$$h_k(s) = \omega_c \frac{(s^2 + 2\zeta_k\omega_k s + \omega_k^2)^2}{(s^2 + 2\delta_k\zeta_k\omega_k s + \omega_k^2)^2(\omega_{c,k} + s)} \tag{4.2.6}$$

for each DOF. This is a notch filter, with center frequency ω_k and the wave model resonance and notch width is given by $\delta_k \geq 1$, in series with a low-pass filter that guarantees a certain roll-off for frequencies larger than $\omega_{c,k}$. ζ_i is the relative damping. $k = 1, ..., 3$, represents the 3 DOFs and represent North, East and heading respectively. For good performance, $\omega_{c,k}$ should be larger than ω_k, that is $\omega_{c,k} > \omega_k$.

4.3 Simple Observer

The first observer proposed in this thesis is originally an attitude observer, recently proposed in Hua (2010). It makes use of accelerometer, magnetometer and linear velocity measurements to generate estimates of attitude and position. For the intended application in this thesis, the observer can be simplified by discarding the attitude estimation part and only consider the position and velocity estimation. The observer will now utilize linear acceleration measurements as input, as well as GPS velocity, heading and position measurements to correct deviations.

4.3.1 Observer Design

Let the body-fixed acceleration measurements delivered by the IMU be denoted $\boldsymbol{f}^b_{imu}$, and the Earth-fixed GPS position and velocity $\boldsymbol{p}^n_{gps}$ and $\boldsymbol{v}^n_{gps}$, respectively. With the attitude estimation removed, the observer equations are

$$\dot{\hat{\boldsymbol{p}}}^n_{b/n} = \boldsymbol{v}^n_{b/n} + \boldsymbol{k}_{pos}(\boldsymbol{p}^n_{gps} + \hat{\boldsymbol{p}}^n_{b/n}) \tag{4.3.1}$$

$$\dot{\hat{\boldsymbol{v}}}^n_{b/n} = Q\boldsymbol{f}^b_{imu} + \boldsymbol{k}_{vel}(\boldsymbol{v}^n_{gps} + \hat{\boldsymbol{v}}^n_{b/n}) \tag{4.3.2}$$

$$\dot{Q} = \boldsymbol{k}_Q(\boldsymbol{v}^n_{gps} + \hat{\boldsymbol{v}}^n_{b/n})(\boldsymbol{f}^b_{imu})^T - \rho Q \tag{4.3.3}$$

$$\rho = \boldsymbol{k}_{norm} max(0, \|Q\| - \sqrt{3}) \tag{4.3.4}$$

where $\boldsymbol{k}_{pos}$, $\boldsymbol{k}_{vel}$,$\boldsymbol{k}_{norm}$, $\boldsymbol{k}_Q \in \mathbb{R}^{3\times3}$ are all some positive constant observer gain matrices, $Q \in \mathbb{R}^{3\times3}$ is a virtual matrix allowing estimation of the specific acceleration in the NED frame. It is not a rotation matrix, but still such that $Q\boldsymbol{f}^b_{imu} - R^n_b\boldsymbol{f}^b_{imu}$ tends to zero. $\|Q\|$ is the Frobenius norm, i.e. $\|Q\| = \sqrt{tr(Q^TQ)}$. In other words, $Q\boldsymbol{f}^b_{imu} + k_{vel}(\boldsymbol{v}^n_{gps} + \hat{\boldsymbol{v}}^n_{b/n})$ can be viewed as an estimate of $\boldsymbol{f}^n$.

This observer does not provide any bias estimation and the measurements have to be filtered through an external wave filter to remove the WF motion before they enter the observer. Stability analysis of the observer state semi-global convergence, see Hua (2010) for details.

4.3.2 Observer Tuning

One of the advantages with this observer is the relatively easy tuning procedure. The observer gain matrices $\boldsymbol{k}_{pos}$, $\boldsymbol{k}_{vel}$, $\boldsymbol{k}_{norm}$, $\boldsymbol{k}_{Q}$ have to be diagonal with only constant positive gains on the diagonal, in order for the observer to satisfy semi-global stability. The constant gains can be found through trial and error.

4.4 Model Based Observer

The observer proposed in this section has a more advanced design than the observer from the previous section. This observer is based on a low-frequency 3 DOF vessel model and incorporates bias estimation and the wave filtering is a part of the observer design. The observer was first developed in Lindegaard (2003), and it is an extension of the observer derived in Fossen and Strand (1999). The extension done in Lindegaard (2003) enables the operator to utilize both velocity and acceleration measurements in the state estimation. The wave models for the position, velocity and acceleration are considered separately i.e. each of the measurements have its own wave filter .

4.4.1 Low-Frequency Ship Model

For DP operations, only movement in the horizontal plane is of interest and a 3 DOF LF vessel model is therefore considered. By simplifying the 6 DOF vessel model described in equations 3.3.1 and 3.3.2, the Viknes 830 can described by the following 3 DOF low frequency model

$$\dot{\boldsymbol{\eta}} = \boldsymbol{R}(\psi_y)\boldsymbol{\nu} \tag{4.4.1}$$

$$\dot{\boldsymbol{b}} = -\boldsymbol{T}_b^{-1}\boldsymbol{b} + \boldsymbol{E}_b\boldsymbol{w}_b \tag{4.4.2}$$

$$\boldsymbol{M}\dot{\boldsymbol{\nu}} + \boldsymbol{D}\boldsymbol{\nu} = \boldsymbol{\tau} + \boldsymbol{R}^T(\psi_y)\boldsymbol{b} \tag{4.4.3}$$

Here, $\boldsymbol{\tau} \in \mathbb{R}^3$ is the applied thruster force, $\boldsymbol{M} = \boldsymbol{M}^T > 0$ is the sum of rigid body mass and hydrodynamical added mass, $\boldsymbol{D} \in \mathbb{R}^{3\times3}$ is the linear damping matrix. All the non-linearities from the 6 DOF model can be combined into a bias term. The bias forces $\boldsymbol{b} \in \mathbb{R}^3$ are modeled as Markov processes with a positive semi-definite diagonal matrix $\boldsymbol{T}_b \in \mathbb{R}^{3\times3}$ of time constants. $\boldsymbol{w}_b \in \mathbb{R}^3$ is a bounded disturbance signal, and $\boldsymbol{E}_b \in \mathbb{R}^{3\times3}$ is a gain factor. The model is expressed in the Earth- and body-fixed coordinate frames. The principal axes of the vessel and the body-fixed frame coincide and it is rotated an angle ψ_y, which is the measured

heading, with respect to the Earth-fixed frame. The transformation between the two coordinate frames can be represented as a rotation matrix

$$\boldsymbol{R}(\psi_y) = \begin{bmatrix} cos\psi_y & -sin\psi_y & 0 \\ sin\psi_y & cos\psi_y & 0 \\ 0 & 0 & 1 \end{bmatrix} \tag{4.4.4}$$

The vectors $\boldsymbol{\eta} = \begin{bmatrix} x & y & \psi \end{bmatrix}^T$ and $\boldsymbol{\nu} = \begin{bmatrix} u & v & r \end{bmatrix}^T$ contains the Earth-fixed position and heading, and the body-fixed velocities respectively. In the following the commutation property between the Earth-fixed parameters and the rotation $\boldsymbol{R}(\alpha)$.

Property 4.1. A matrix $\boldsymbol{A} \in \mathbb{R}^{3\times 3}$ is said to commute with the rotation $\boldsymbol{R}(\alpha)$ if

$$\boldsymbol{A}\boldsymbol{R}(\alpha) = \boldsymbol{R}(\alpha)\boldsymbol{A} \tag{4.4.5}$$

Matrices that satisfy Property 4.1 are linear combinations $\boldsymbol{A} = a_1\boldsymbol{R}(\theta) + a_2\boldsymbol{I} + a_3\boldsymbol{k}^T\boldsymbol{k}$ for scalars a_i, θ and $\boldsymbol{k} = \begin{bmatrix} 0 & 0 & 1 \end{bmatrix}^T$, the axis of rotation. Since $\boldsymbol{R}(\alpha)$ is orthogonal, that is $\boldsymbol{R}^T(\alpha) = \boldsymbol{R}^{-1}(\alpha)$, Property 4.1 implies that

$$\boldsymbol{A} = \boldsymbol{R}^T(\alpha)\boldsymbol{A}\boldsymbol{R}(\alpha) = \boldsymbol{R}(\alpha)\boldsymbol{A}\boldsymbol{R}^T(\alpha) \tag{4.4.6}$$

Also, if $\boldsymbol{A}$ is non singular, $\boldsymbol{A}^{-1}$ commutes with $\boldsymbol{R}(\alpha)$, that is

$$\boldsymbol{A}\boldsymbol{R}(\alpha) = \boldsymbol{R}(\alpha)\boldsymbol{A} \iff \boldsymbol{A}^{-1}\boldsymbol{R}(\alpha) = \boldsymbol{R}(\alpha)\boldsymbol{A}^{-1} \tag{4.4.7}$$

4.4.2 Complete Ship and Environmental Model

As mentioned, the observer will consider the wave models for position, velocity and acceleration separately. This gives us three wave models.

$$\dot{\boldsymbol{p}}_w = \boldsymbol{A}_{pw}\boldsymbol{p}_w + \boldsymbol{E}_{pw}\boldsymbol{w}_{pw} \tag{4.4.8}$$
$$\dot{\boldsymbol{v}}_w = \boldsymbol{A}_{vw}\boldsymbol{v}_w + \boldsymbol{E}_{vw}\boldsymbol{w}_{vw} \tag{4.4.9}$$
$$\dot{\boldsymbol{a}}_w = \mathbf{A}_{aw}\boldsymbol{a}_w + \boldsymbol{E}_{aw}\boldsymbol{w}_{aw} \tag{4.4.10}$$

In general, the order of each model can be chosen arbitrary, but in this thesis, fourth order models are chosen for the position and heading, velocity and acceleration measurements. This gives us $\boldsymbol{p}_w \in \mathbb{R}^{12}$, $\boldsymbol{v}_w \in \mathbb{R}^{12}$ and $\boldsymbol{a}_w \in \mathbb{R}^8$, which

describe the wave induced position, velocity and acceleration respectively. The matrices $\boldsymbol{A}_{pw} \in \mathbb{R}^{12\times12}$, $\boldsymbol{A}_{vw} \in \mathbb{R}^{12\times12}$, $\boldsymbol{A}_{aw} \in \mathbb{R}^{8\times8}$ are assumed Hurwitz and describe the first order wave induced motion. The wave and bias models are driven by disturbances of appropriate dimensions. Note that the bias time constant matrix $\boldsymbol{T}_b$ and each 3×3 sub-block of $\boldsymbol{A}_{pw}$ satisfy Property 4.1.

The Earth-fixed states and the body-fixed states are collected in $\mathbf{x}_1 = \begin{bmatrix} \boldsymbol{p}_w^T & \boldsymbol{\eta}^T & \boldsymbol{b}^T \end{bmatrix}^T$ and $\boldsymbol{x}_2 = \begin{bmatrix} \boldsymbol{v}_w^T & \boldsymbol{a}_w^T & \boldsymbol{\nu}^T \end{bmatrix}^T$ respectively. The dimensions are $\boldsymbol{x}_1 \in \mathbb{R}^{18}$ and $\boldsymbol{x}_2 \in \mathbb{R}^{23}$. The state vectors $\boldsymbol{x}_1$ and $\boldsymbol{x}_2$ are now combined into a new vector $\boldsymbol{x} = \begin{bmatrix} \boldsymbol{x}_1^T & \boldsymbol{x}_2^T \end{bmatrix}^T$. Now a block diagonal transformation matrix $T : \mathbb{R} \to \mathbb{R}^{42\times42}$ is defined

$$\boldsymbol{T}(\psi_y) = Diag(\boldsymbol{R}^T(\psi_y), \ldots, \boldsymbol{R}^T(\psi_y), \boldsymbol{I}_{23}) \tag{4.4.11}$$

By using all of the above, the combined environment and LF ship model can be written on compact form

$$\dot{\boldsymbol{x}} = \boldsymbol{T}^T(\psi_y)\boldsymbol{A}\boldsymbol{T}(\psi_y)\boldsymbol{x} + \boldsymbol{B}\boldsymbol{\tau} + \boldsymbol{E}\boldsymbol{w} \tag{4.4.12}$$

The matrices in 4.4.12 has the following structure

$$\boldsymbol{A} = \begin{bmatrix} \boldsymbol{A}_{pw} & 0 & 0 & 0 & 0 & 0 \\ 0 & 0 & 0 & 0 & 0 & I \\ 0 & 0 & -\boldsymbol{T}_b^{-1} & 0 & 0 & 0 \\ 0 & 0 & 0 & \boldsymbol{A}_{vw} & 0 & 0 \\ 0 & 0 & 0 & 0 & \boldsymbol{A}_{aw} & 0 \\ 0 & 0 & \boldsymbol{M}^{-1} & 0 & 0 & -\boldsymbol{M}^{-1}\boldsymbol{D} \end{bmatrix}$$

$$\boldsymbol{B} = \begin{bmatrix} 0 \\ 0 \\ 0 \\ 0 \\ 0 \\ \boldsymbol{M}^{-1} \end{bmatrix}, \quad \boldsymbol{E} = \begin{bmatrix} \boldsymbol{E}_{pw} & 0 & 0 & 0 \\ 0 & 0 & 0 & 0 \\ 0 & \boldsymbol{E}_b & 0 & 0 \\ 0 & 0 & \boldsymbol{E}_{vw} & 0 \\ 0 & 0 & 0 & \boldsymbol{E}_{aw} \\ 0 & 0 & 0 & 0 \end{bmatrix} \tag{4.4.13}$$

Measurements

Position and heading measurements are always required. The number of velocity measurements and acceleration measurements utilized are 3 and 2 respectively. We get $\boldsymbol{y}_1 \in \mathbb{R}^3$, $\boldsymbol{y}_2 \in \mathbb{R}^3$, $\boldsymbol{y}_3 \in \mathbb{R}^2$, and define the measurements:

$$\boldsymbol{y}_1 = \boldsymbol{\eta} + \mathbf{C}_{pw}\boldsymbol{p}_w \tag{4.4.14}$$
$$\boldsymbol{y}_2 = \boldsymbol{\Gamma}_2\boldsymbol{\nu} + \boldsymbol{C}_{vw}\boldsymbol{v}_w \tag{4.4.15}$$
$$\boldsymbol{y}_3 = \boldsymbol{\Gamma}_3\dot{\boldsymbol{\nu}} + \boldsymbol{C}_{aw}\boldsymbol{a}_w \tag{4.4.16}$$

where $\boldsymbol{\Gamma}_2$ and $\boldsymbol{\Gamma}_3$ are projections isolating the components of the LF-model that are actually measured. In practice this lets the operator choose what measurements to use in the state estimation. The system 4.4.14 - 4.4.16 can be written compactly

$$\mathbf{y} = \boldsymbol{C}_y(\psi_y)\boldsymbol{x} + \boldsymbol{D}_y\boldsymbol{\tau} \tag{4.4.17}$$

where

$$\boldsymbol{C}_y(\psi_y) = \begin{bmatrix} \boldsymbol{C}_{pw} & \boldsymbol{I} & \mathbf{0} & \mathbf{0} & \mathbf{0} & \mathbf{0} \\ \mathbf{0} & \mathbf{0} & \mathbf{0} & \boldsymbol{C}_{vw} & \mathbf{0} & \boldsymbol{\Gamma}_2 \\ \mathbf{0} & \mathbf{0} & -\boldsymbol{\Gamma}_3\boldsymbol{M}^{-1}\boldsymbol{R}^T & 0 & \boldsymbol{C}_{aw} & -\boldsymbol{\Gamma}_3\boldsymbol{M}^{-1}\boldsymbol{D} \end{bmatrix} \tag{4.4.18}$$

$$\boldsymbol{D}_y = \begin{bmatrix} \mathbf{0} & \mathbf{0} & \boldsymbol{M}^{-T}\boldsymbol{\Gamma}_3^T \end{bmatrix}^T \tag{4.4.19}$$

4.4.3 Observer Design

By duplicating the LF model from the and introducing a low-pass filter in order to achieve a certain roll-off effect, the following model based observer is proposed

$$\dot{\boldsymbol{a}}_f = \boldsymbol{T}_f^{-1}(-\boldsymbol{a}_f + \tilde{\boldsymbol{y}}_3) \tag{4.4.20}$$

$$\dot{\hat{\boldsymbol{x}}} = \boldsymbol{T}^T(\psi_y)\boldsymbol{A}\boldsymbol{T}(\psi_y)\hat{\boldsymbol{x}} + \boldsymbol{B}\boldsymbol{\tau} + \boldsymbol{K}(\psi_y)\tilde{\boldsymbol{y}} + \boldsymbol{K}_f\boldsymbol{a}_f \tag{4.4.21}$$

and the estimated output

$$\hat{\boldsymbol{y}} = \boldsymbol{C}_y(\psi_y)\hat{\boldsymbol{x}} + \boldsymbol{D}_y\boldsymbol{\tau} \tag{4.4.22}$$

The estimation error is given by $\tilde{\boldsymbol{x}} = \mathbf{x} - \hat{\boldsymbol{x}}$ and the output error is $\tilde{\boldsymbol{y}} = \boldsymbol{C}_y(\psi_y)\tilde{\boldsymbol{x}}$. To reduce the number of interconnections, the observer gain matrices are chosen to be

$$\boldsymbol{K}(\psi_y) = \begin{bmatrix} \boldsymbol{K}_{11} & \boldsymbol{0} & \boldsymbol{0} \\ \boldsymbol{K}_{21} & \boldsymbol{0} & \boldsymbol{0} \\ \boldsymbol{K}_{31} & \boldsymbol{0} & \boldsymbol{0} \\ \boldsymbol{0} & \boldsymbol{K}_{42} & \boldsymbol{0} \\ \boldsymbol{0} & \boldsymbol{0} & \boldsymbol{K}_{53} \\ \boldsymbol{K}_{62}\boldsymbol{R}^T(\psi_y) & \boldsymbol{K}_{62} & \boldsymbol{0} \end{bmatrix} \tag{4.4.23}$$

$$K_f = \begin{bmatrix} \boldsymbol{0} & \boldsymbol{0} & \boldsymbol{0} & \boldsymbol{0} & \boldsymbol{0} & \boldsymbol{K}_a^T \end{bmatrix}^T \tag{4.4.24}$$

Each and every 3×3 block of $\boldsymbol{K}_{11}$, $\boldsymbol{K}_{21}$ and $\boldsymbol{K}_{31}$ have to commute with the rotation matrix $\boldsymbol{R}(\psi_y)$ (Property 4.1). In (Lindegaard, 2003) it is stated that the observer is uniform global exponentially stable (UGES). For proof and stability analysis, see (Lindegaard, 2003). In figure 4.1, the Simulink block diagram of the observer is shown.

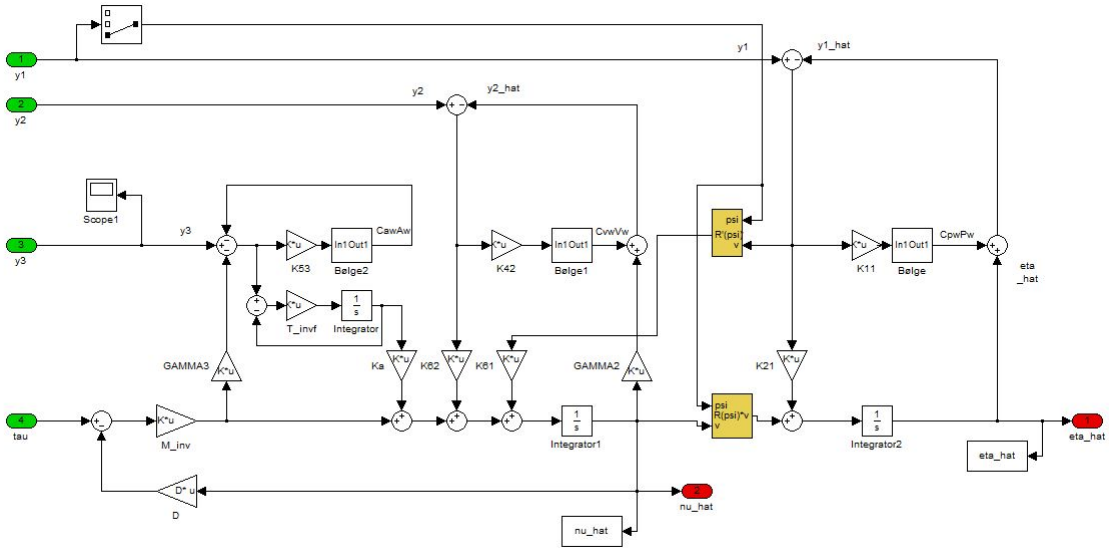

Figure 4.1: Simulink block diagram of the model based observer.

4.4.4 Observer Tuning

To find gains for the position and velocity innovation, pole-placing is used. Since fourth order models are chosen, the tuning rules from Fossen and Strand (1999) does not apply here. Instead, an extension of these rules are proposed.

First, consider the surge dynamics being updated from the position measurements.

$$\frac{\hat{\eta}_k}{y_{1,k}}(s) = h_k(s) \tag{4.4.25}$$

The goal is to find suitable gains $\boldsymbol{K}_{11}$ and $\boldsymbol{K}_{21}$, that gives the desired notch and roll-off. As mentioned, this is being done one DOF at a time by defining $\alpha_{p,k} = \omega_{p,k}^2 > 0$ and $\beta_{p,k} = 2\zeta_{p,k}\omega_{p,k} > 0$ and letting

$$\boldsymbol{A}_{pw,k} = \begin{bmatrix} 0 & 1 & 0 & 0 \\ -\alpha_{p,k} & -\beta_{p,k} & 0 & 1 \\ 0 & 0 & 0 & 1 \\ 0 & 0 & -\alpha_{p,k} & -\beta_{p,k} \end{bmatrix} \tag{4.4.26}$$

$$\boldsymbol{C}_{pw,k} = \begin{bmatrix} 1 & 0 & 0 & 0 \end{bmatrix} \tag{4.4.27}$$

and selecting observer gains according to

$$\boldsymbol{k}_{11,k} = \boldsymbol{L}_k^{-1}\boldsymbol{c}_k \tag{4.4.28}$$

$$k_{21,k} = \omega_{c,k} \tag{4.4.29}$$

where

$$\boldsymbol{L}_k = \begin{bmatrix} 1 & 0 & 0 & 0 \\ 2\beta_{p,k} & 1 & 0 & 0 \\ \alpha_{p,k} + \beta_{p,k}^2 & \beta_{p,k} & 0 & 1 \\ \beta_{p,k} & 1 & -1 & 0 \end{bmatrix} \tag{4.4.30}$$

$$\boldsymbol{c}_k = \begin{bmatrix} 2\beta_{p,k}(\delta_{p,k} - 1) \\ \beta_{p,k}^2(\delta_{p,k}^2 - 1) + 2\beta_{p,k}(\delta_{p,k} - 1)\omega_{c,k} \\ \alpha_{p,k}\beta_{p,k}(\delta_{p,k} - 1) + \beta_{p,k}^2(\delta_{p,k}^2 - 1)\omega_{c,k} \\ 2\beta_{p,k}(\delta_{p,k} - 1)\omega_{c,k} \end{bmatrix} \tag{4.4.31}$$

This choice of gains ensures that the specified notch-effect and roll-off is acquired. The gains $\boldsymbol{K}_{31}$ and $\boldsymbol{K}_{61}$, the gains used to update the bias and LF velocity, can be selected freely. For the velocity measurements, the exact same approach can be applied to assign values to $\boldsymbol{K}_{42}$ and $\boldsymbol{K}_{62}$.

As mentioned, the observer possesses the feature of using measured acceleration in the state estimation as well. The gain $\boldsymbol{K}_f$ serves as a weighting gain that determines how much emphasis should be put on the model. If $\boldsymbol{K}_f = 0$ then the

measured acceleration is not utilized at all. For $\boldsymbol{K}_f = 1$, the LF model description is completely disregarded for low-frequencies.

The roll-off is taken care of by the low-pass filter between the innovation $\tilde{\boldsymbol{y}}_{\boldsymbol{3}}$ and $\dot{\hat{\boldsymbol{\nu}}}$. The filter constants $\boldsymbol{T}_f$ should therefore be selected as

$$\boldsymbol{T}_f^{-1} = diag(\omega_{c,1}, ..., \omega_{c,n_{y_3}}) \tag{4.4.32}$$

To obtain the desired notch-effect around the resonance frequency, select

$$\boldsymbol{K}_{53} = \begin{bmatrix} \mathbf{0} \\ diag(\delta_{a,1}, ..., \delta_{a,n_{y_3}}) \end{bmatrix} \tag{4.4.33}$$

Chapter 5

Simulation

5.1 Introduction

When introducing new features to a system, it is crucial that they work properly. If any of the new components have a malfunction, or in some way causes other components to fail, not only is the entire system in risk of being damaged, but in worst case human lives could be lost. Because of this, it is important to test and verify all functions and features in a simulator before installing them on a live system. Testing in a simulator can reveal software bugs and other design flaws, that otherwise would not have been discovered before they were implemented on a live system.

The Viknes 830 owned by MR is already a working USV, and the DP system developed in Kjerstad (2010) have been tested thoroughly. In chapter 3 a Viknes 830 simulator was introduced. The simulator was also developed in Kjerstad (2010) for the sole purpose of testing the DP control system. This thesis will also use this simulator to test the proposed observers, and to verify that they in fact give satisfactory results. Especially the degree of wave filtering being done is of interest. In the following sections a simulator setup will be presented, and the proposed observers will be tested.

All models presented in this thesis, the 6 DOF vessel model, the environmental disturbances, the DP controller, actuators and both observers are implemented in Simulink and Matlab, and combined they constitute a Viknes 830 simulator. As mentioned, many blocks are directly adapted from the MSS toolbox developed by Marinecontrol.org.

5.2 Test Scenarios

To test the observers some simulation scenarios have to be determined. Two scenarios will be proposed, and since the observers wave-handling is of most interest, each scenario will have different wave and wind characteristics. The ocean current is of less interest and will of practical reasons remain the same in both scenarios. In addition, the desired position i.e. the DP system set point, will be the same for comparison reasons. To make the environmental influence as realistic as possible, the wave and wind parameters will be set according to the Beaufort wind force scale explained in chapter 3.

In both scenarios the desired position will be set to 60 [m] and 10 [deg] in front of the vessel. The virtual pendulum line i.e. the radius of the pendulum, is set to 10 [m]. As mentioned, the DP system implemented has the capability of both WOHC and WOPC. Since the choice of DP controller does not affect the observer performance, WOPC is chosen. The ocean current is of little interest in these simulations and could be omitted, but to get a more realistic scenario, a weak current is imposed on the vessel. The ocean current is set to 0.1 [m/s] at a 90 [deg] angle i.e. a current coming from East, hitting the port side of the USV in its initial position. The simulation time is set to 400 [s]. Two scenarios will be proposed in the following. One scenario with relatively small waves, and one scenario with relatively large waves. The described scenarios are in the opposite ends of the scale. The first scenario is a plausible scenario that the USV can encounter when operating near shore and in places where the USV are intended to operate. The second scenario however, is highly unlikely for the USV to experience. These conditions are chosen to get a better understanding of how the wave filtering works, and how the performance of the DP system is affected by waves, with and without wave filtering.

5.2.1 Calm Sea Conditions

The first test scenario corresponds to sea state 2 in the Beaufort wind force scale. The significant wave height is set to 0.5 [m], and the wind speed is set to 1.3 [m/s]. Both wind and waves are set to 90 [deg] direction. For a small vessel, like the USV, 0.5 [m] wave height is actually relatively large. The reason why even smaller waves is not considered is because the effect of the wave filter will not be noticeable.

Figure 5.1 shows the vessel trajectory towards the position set point with the given configuration. Clearly, the waves create fluctuations in the position measurements, making the vessel trajectory non-smooth. Due to the oscillatory motion of the waves, the vessel is pushed back and forth, creating small deviations from the

desired trajectory. This also affects the amount of work done by the controller and actuators. In 5.2 the DP controller set-points are shown.

Notice how the throttle is fairly constant until the vessel reaches the desired position, and that it works in small bursts to keep the vessel at the desired position. Because of the WF motion, the tunnel thruster controller has to constantly correct the heading, as can be seen in figure 5.2. The rudder is not utilized at all in this scenario, suggesting that the relative water speed never exceed 1 [m/s].

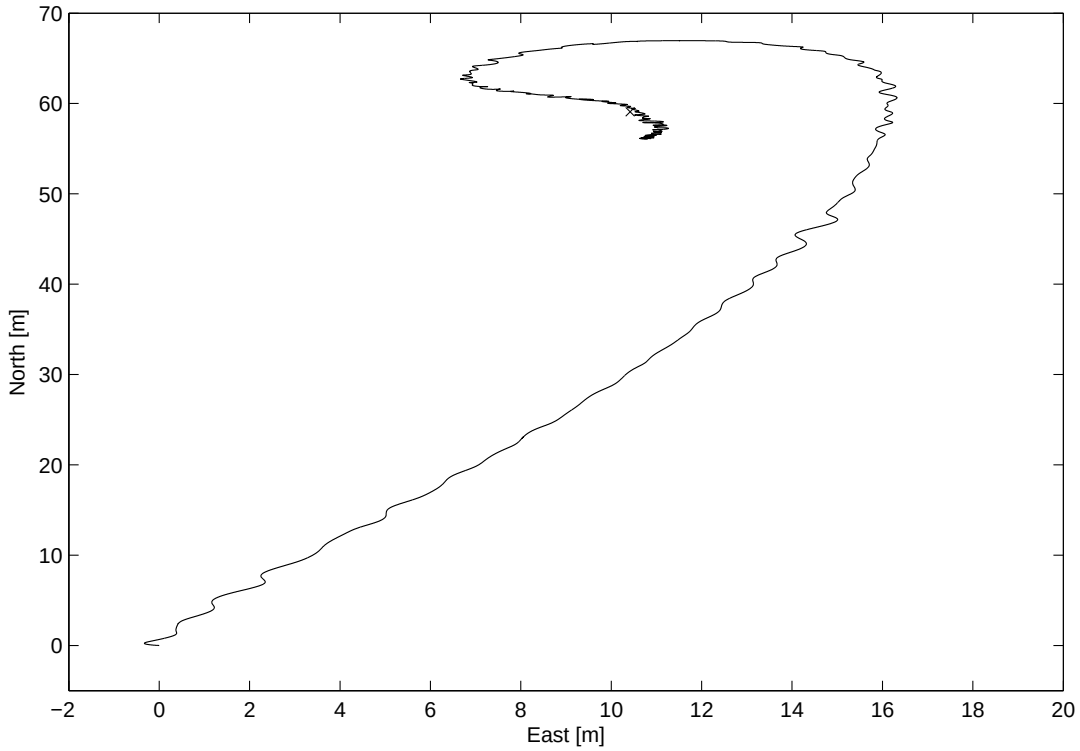

Figure 5.1: A reference run. The vessel trajectory towards the desired position.

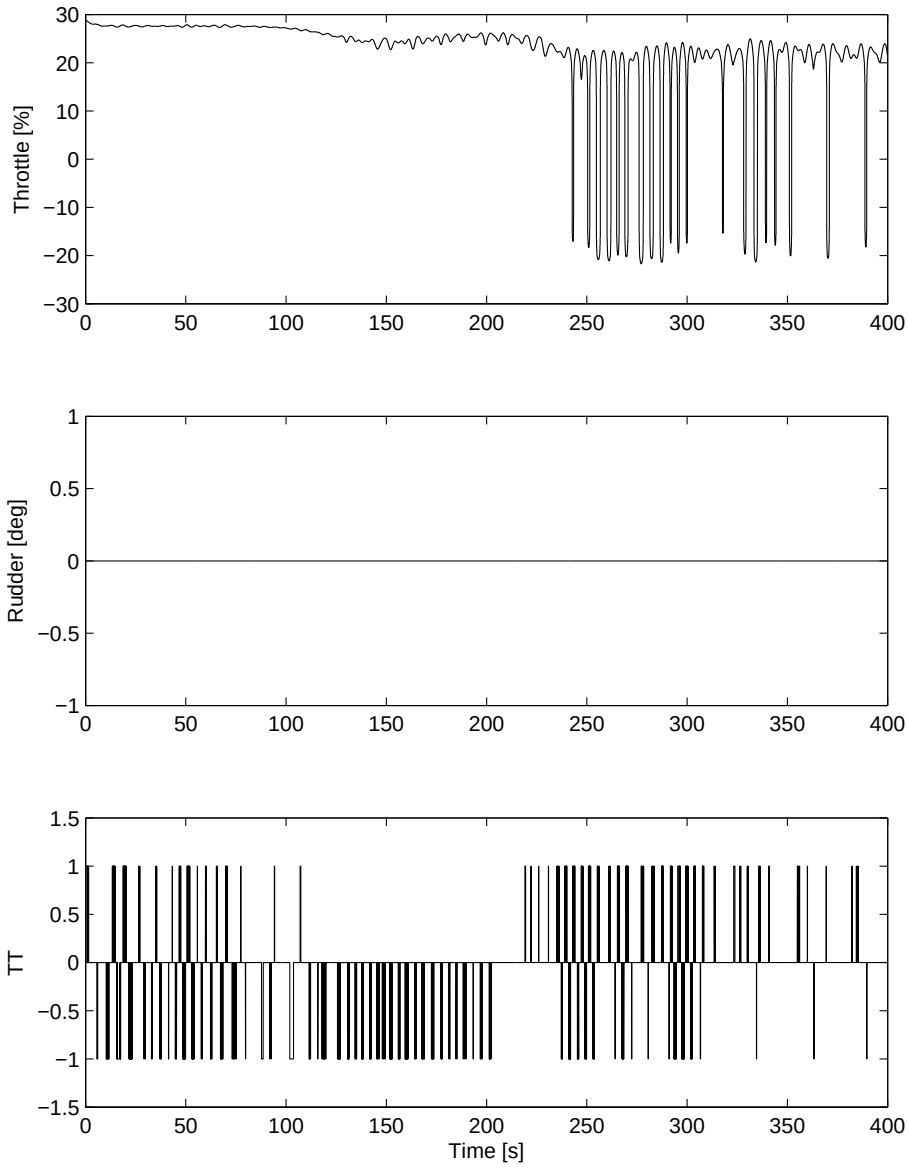

Figure 5.2: The DP controller set-points.

5.2.2 Rough Sea Conditions

In the second scenario, the wave height is increased significantly. On the Beaufort wind force scale a wave height of 4 [m] corresponds to a 6, which is classified as "rough" sea. For the the USV this is relatively large waves. A 6 on the Beafort wind force scale corresponds to a wind speed of 4.3 [m/s] to 5.5 [m/s], but due to the shape of the vessel and the fact the Viknes is not stable when its heading is towards the wind, the wind speed had to be modified to 3 [m/s]. The other simulation parameters were the same as in the first test scenario. Figure 5.3 shows the trajectory of the vessel in this sea state.

Again, the trajectory is very non-smooth, and it can be seen on the set-points that the controller has to work hard in order to get the vessel to, and to keep the vessel at the desired position. Because the size of the waves are much bigger in this case, the fluctuations are more noticeable. The throttle and tunnel thruster has approximately the same behavior as earlier, but notice that the rudder is now active in small periods of time. The controller set-points in rough weather are shown in figure 5.4.

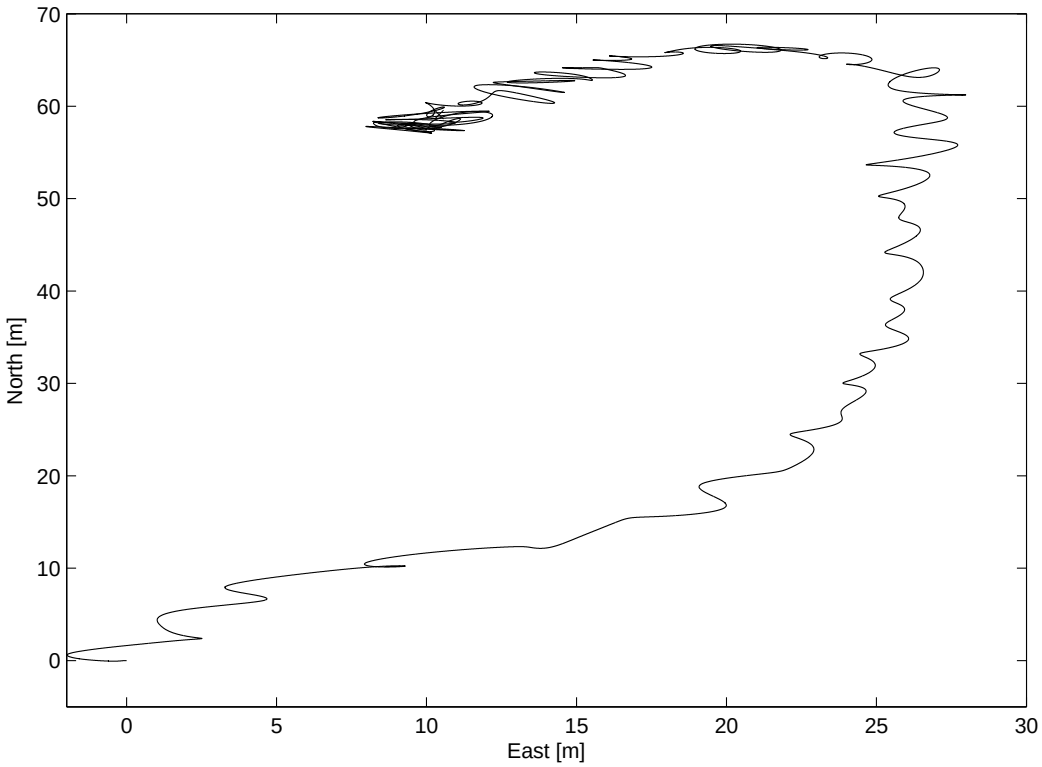

Figure 5.3: Reference run. Rough sea state.

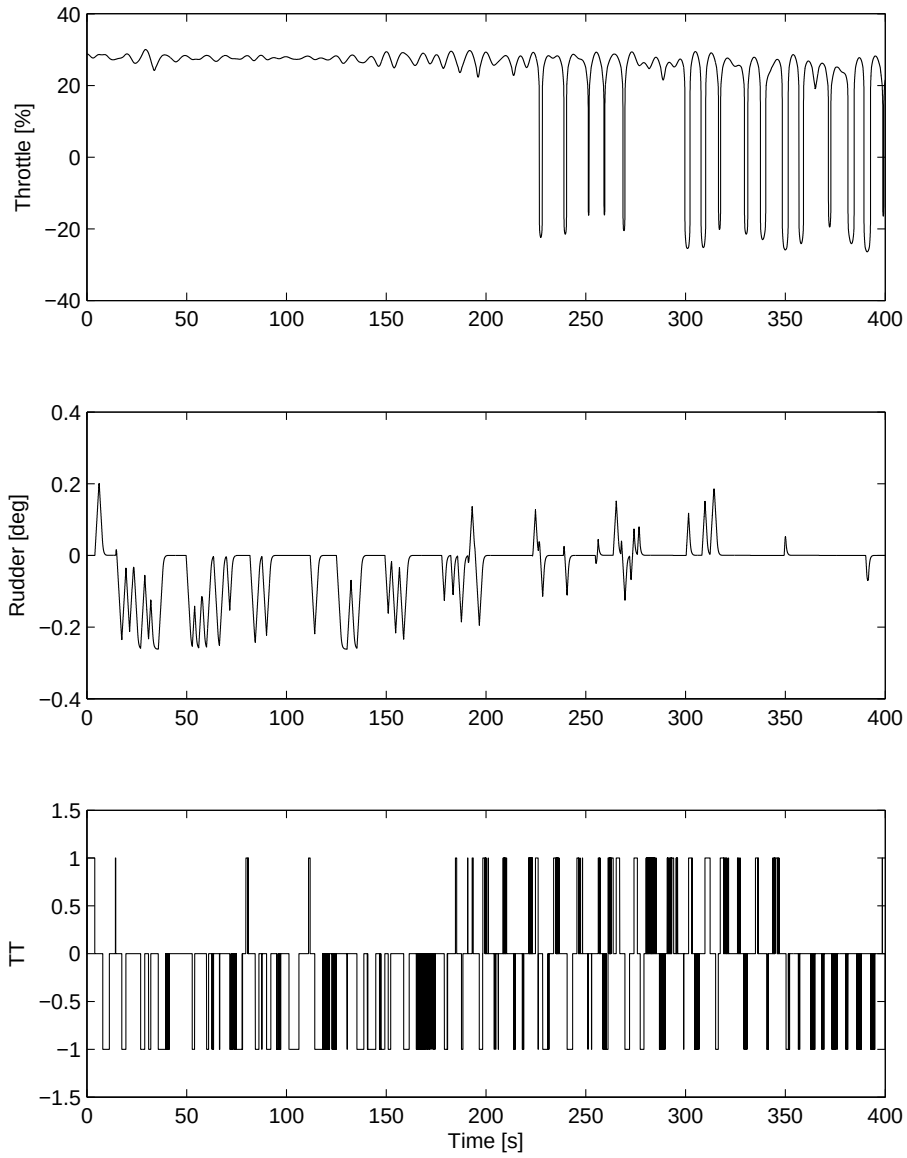

Figure 5.4: DP controller set-points in rough sea.

5.3 Vessel Parameters

In Kjerstad (2010) all simulator parameters were found through experiments and testing. The vessels hydrodynamical characteristics were found using a hydrodynamical software called ShipX VERES. The following sections will present all parameters used in the simulations. Most parameters are directly adapted from Kjerstad (2010), except observer and controller tuning parameters.

5.3.1 6 DOF Vessel Parameters

The vessel matrices $\mathbf{M}, \mathbf{C}^*_{RB}, \mathbf{C}^*_A$and $\mathbf{D}_L$was found to be:

$$\mathbf{M} = \begin{bmatrix} 5442.3 & 0 & 0 & 0 & -1260.7 & 0 \\ 0 & 6776.8 & 0 & 2318.5 & 0 & 400.6 \\ 0 & 0 & 18725.4 & 0 & 3737.4 & 0 \\ 0 & 2104.4 & 0 & 6411.3 & 0 & 198.7 \\ -1260.7 & 0 & 7605.1 & 0 & 56688.7 & 0 \\ 0 & 361.5 & 0 & 106.8 & 0 & 24394.5 \end{bmatrix} \tag{5.3.1}$$

$$\mathbf{C}^*_{RB} = U \begin{bmatrix} 0 & 0 & 0 & 0 & 0 & 0 \\ 0 & 0 & 0 & 0 & 0 & 5002.6 \\ 0 & 0 & 0 & 0 & -5002.6 & 0 \\ 0 & 0 & 0 & 0 & 0 & 1260.7 \\ 0 & 0 & 0 & 0 & 0 & 0 \\ 0 & 0 & 0 & 0 & 0 & 0 \end{bmatrix} \tag{5.3.2}$$

$$\mathbf{C}^*_A = U \begin{bmatrix} 0 & 0 & 0 & 0 & 0 & 0 \\ 0 & 0 & 0 & 0 & 0 & 0.17 \\ 0 & 0 & 0 & 0 & -1.37 & 0 \\ 0 & 0 & 0 & 0 & 0 & 0.08 \\ 0 & 0 & 0 & 0 & -0.76 & 0 \\ 0 & 0 & 0 & 0 & 0 & 0.03 \end{bmatrix} \tag{5.3.3}$$

$$\mathbf{D}_L = diag\{268.09, 1083.3, 0, 84.3, 0, 1274.2\} \tag{5.3.4}$$

The nonlinear surge damping was found by curve fitting and is approximately

$$X \approx 11499 \left(\frac{0.075}{(log_{10} R_n - 2)^2} + 0.0025 \right) |u_r| \, u_r \tag{5.3.5}$$

The cross flow drag was calculated to be

$$Y \approx 143.7 \int_{-\frac{Lpp}{2}}^{\frac{Lpp}{2}} |v_r + xr| (v_r + xr) dx \tag{5.3.6}$$

$$N \approx 143.7 \int_{-\frac{Lpp}{2}}^{\frac{Lpp}{2}} x |v_r + xr| (v_r + xr) dx \tag{5.3.7}$$

and the integration was done by the simulator. The restoring forces matrix $\mathbf{G}$ was calculated to be

$$\mathbf{G} = \begin{bmatrix} 0 & 0 & 0 & 0 & 0 & 0 \\ 0 & 0 & 0 & 0 & 0 & 0 \\ 0 & 0 & 146197.67 & 0 & -9002,86 & 0 \\ 0 & 0 & 0 & 47648.48 & 0 & 0 \\ 0 & 0 & -9002.86 & 0 & 423188.66 & 0 \\ 0 & 0 & 0 & 0 & 0 & 0 \end{bmatrix} \tag{5.3.8}$$

The fluid memory effects was computed entirely in software and consisted of 18 independent linear systems, each given by equations 3.3.15 and 3.3.16.

5.3.2 Actuators

The main propulsion engine dynamics was assumed to be

$$\dot{\omega}_a = 2(-\omega_a + \omega_d) \tag{5.3.9}$$

where ω_a is the actual engine RPM. The propeller model was found to be

$$X_p = 29.37n |n| - 6.12 |n| u_a \tag{5.3.10}$$

here, n is the propeller shaft angular velocity which can be found by

$$n = \frac{2.03\omega_a}{60} \tag{5.3.11}$$

The rudder and tunnel thruster dynamics was decided to be

$$\dot{\delta}_a = 2(-\delta_a + \delta) \tag{5.3.12}$$

and

$$\dot{\alpha} = 50(-\alpha + \alpha_d(C_{TT})) \tag{5.3.13}$$

respectively. The conversion from the given tunnel thruster force to the control signal C_{TT} were done in a Matlab *function* block. The forces and moments generated by the rudder and tunnel thruster can be summarized

$$X_r = 77.5v_r\left(8.64\frac{\delta^2}{\pi} + 0.0135\right) \tag{5.3.14}$$

$$Y_r = 205v_r^2\delta \tag{5.3.15}$$

$$K_r = -183.5v_R^2\delta \tag{5.3.16}$$

$$N_r = -717.4v_r^2\delta \tag{5.3.17}$$

$$N_{TT} = 29.43\alpha \tag{5.3.18}$$

The vessel parameters above was mostly calculated by a hydrodynamical software. To validate the model, real world data was compared with the simulator data. Some errors were found, but due to limited time for data gathering, the parameters was accepted, see Kjerstad (2010) for a more detailed discussion.

5.3.3 Environmental Forces

Most of the environmental forces were implemented by Simulink components found in the hydro library in Marinecontrol.org (2009), and the details of these calculations is therefore left out of this thesis. A detailed explanation is left to Kjerstad (2010).

5.3.4 DP Controller

The suspension point controller was set up to be

$$\dot{\psi}_d = k(\epsilon)(-\psi_d + \psi_c) \tag{5.3.19}$$

and the gain $k(\epsilon)$ was defined as

$$k(\epsilon) = \epsilon + 0.004 \tag{5.3.20}$$

and

$$\dot{\epsilon} = 0.05\left(-\epsilon + \left|\dot{\psi}_c\right|\right) \tag{5.3.21}$$

The gains of the WOHC was tuned to

$$K_{d_S} = 1000 \quad (5.3.22)$$
$$K_{i_s} = 10 \quad (5.3.23)$$
$$K_{\psi_R} = 1000 \quad (5.3.24)$$
$$K_{\psi_{TT}} = 1 \quad (5.3.25)$$

5.4 Observer tuning

The proposed observers need some tuning in order to give good state estimates. To get good results, it is important to tune the observer parameters systematically. This is done to get a better understanding of what each observer gain does with the estimates. In addition, the tuning procedure becomes more efficient and redundant tuning is avoided.

In the model based observer the wave filter is incorporated in the observer dynamics, making the tuning procedure more complex, while in the second observer the position, heading and acceleration measurements passes through the wave filter before entering the observer. In the latter case, both the wave filter and the observer needs to be tuned properly. Since each observer is tuned differently, two procedures are explained in the following.

5.4.1 Tuning of Simple Observer

Since the wave filter in this case is outside the observer, parameters for both the wave filter and the observer needs to be chosen. First the wave filter is tuned properly, then the gain matrices can be found:

1. First, the parameters of the notch and low-pass filter needs to be found. First the cut-off frequency, ω_c is chosen to achieve good noise filtering.

2. Next, the "notch" in the wave filter should be determined. Figure 5.5 illustrates in what frequency domain the notch should be placed in order to achieve good wave filtering. The parameters ω_i, δ_i and ζ_i , where $i = 1, ..., 3$, decides the center frequency, the notch width and the damping ratio respectively. Tuning these parameters are mostly based on trial and error, but experience and knowledge will make the process easier.

3. Now the observer gain matrices $\boldsymbol{k}_{pos}$, $\boldsymbol{k}_{vel}$, $\boldsymbol{k}_Q$, $\boldsymbol{k}_{norm}$ can be found through trial and error. Tuning experiments indicated that it was advantageous to

start with $\boldsymbol{k}_{pos}$ and $\boldsymbol{k}_{vel}$, since these gains seemed to have the largest impact on the estimates. A large value on these gains made the estimates more noisy, but they also seemed to follow the measurements better. Small values made the estimates smoother, but they did not follow the measurements in a satisfactory way. The two remaining gain matrices were chosen almost arbitrarily, since they had little or no impact on the estimates.

The resulting observer gains used in the simulations was

$$\boldsymbol{k}_{pos} = \begin{bmatrix} 1.5 & 0 & 0 \\ 0 & 1.5 & 0 \\ 0 & 0 & 1.5 \end{bmatrix}, \ \boldsymbol{k}_{vel} = \begin{bmatrix} 1.1 & 0 & 0 \\ 0 & 1.1 & 0 \\ 0 & 0 & 1.1 \end{bmatrix}$$

$$\boldsymbol{k}_{Q} = \begin{bmatrix} 0.5 & 0 & 0 \\ 0 & 0.5 & 0 \\ 0 & 0 & 0.5 \end{bmatrix}, \ \boldsymbol{k}_{norm} = \boldsymbol{I}$$

and the initial wave filter parameters used was found to be

$$\begin{aligned} \omega_c &= 1.1 \\ \omega_i &= 0.89 \\ \delta_i &= 3 \\ \zeta_i &= 0.1 \end{aligned}$$

5.4.2 Tuning of Model Based Observer

The model based observer was tuned in the following fashion:

1. To get the desired noise reduction, ω_c, the cut-off frequency needs to be chosen. By setting this first, unwanted noise are removed and it is easier to work with the other parameters.

2. When the measurement noise is successfully removed, the notch in the wave filter can be placed. This is done by choosing values for ω_i, δ_i and ζ_i. This is the same procedure as with the model-free observer.

3. The remaining gains can now be set according to the tuning rules proposed in chapter 3.

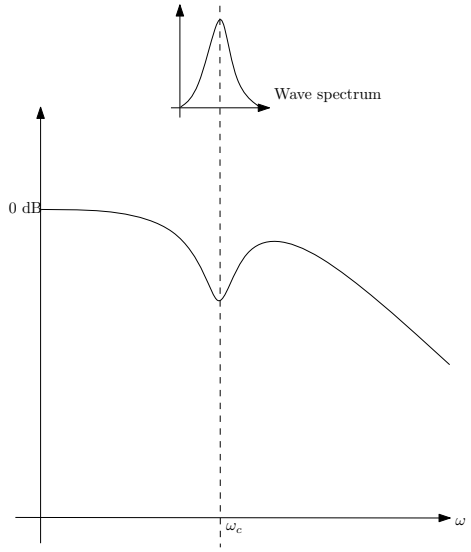

Figure 5.5: The "notch" of the wave filter is placed at the same frequencies as the wave spectrum peak.

The tuning process resulted in the following initial observer configuration.

$$\begin{aligned} \omega_c &= 1.1 \\ \omega_i &= 0.89 \\ \delta_i &= 4 \\ \zeta_i &= 0.1 \end{aligned}$$

These choices of parameters gave good wave and noise filtering. This filter configuration worked satisfactory for all DOFs. The remaining gain matrices were chosen according to the tuning rules from chapter 3, and $\boldsymbol{K}_{61} = \boldsymbol{K}_{31} = \boldsymbol{K}_{21} = \boldsymbol{I}$. The matrix $\boldsymbol{K}_a$, the weighting matrix that decides how much emphasis is put on the acceleration measurement and the model was set to

$$\boldsymbol{K}_a = \begin{bmatrix} 0.5 & 0 \\ 0 & 0.5 \\ 0 & 0 \end{bmatrix} \tag{5.4.1}$$

meaning that equal emphasis is put on model and acceleration measurements. This tuning gave good results for the calm weather scenario.

5.5 Results

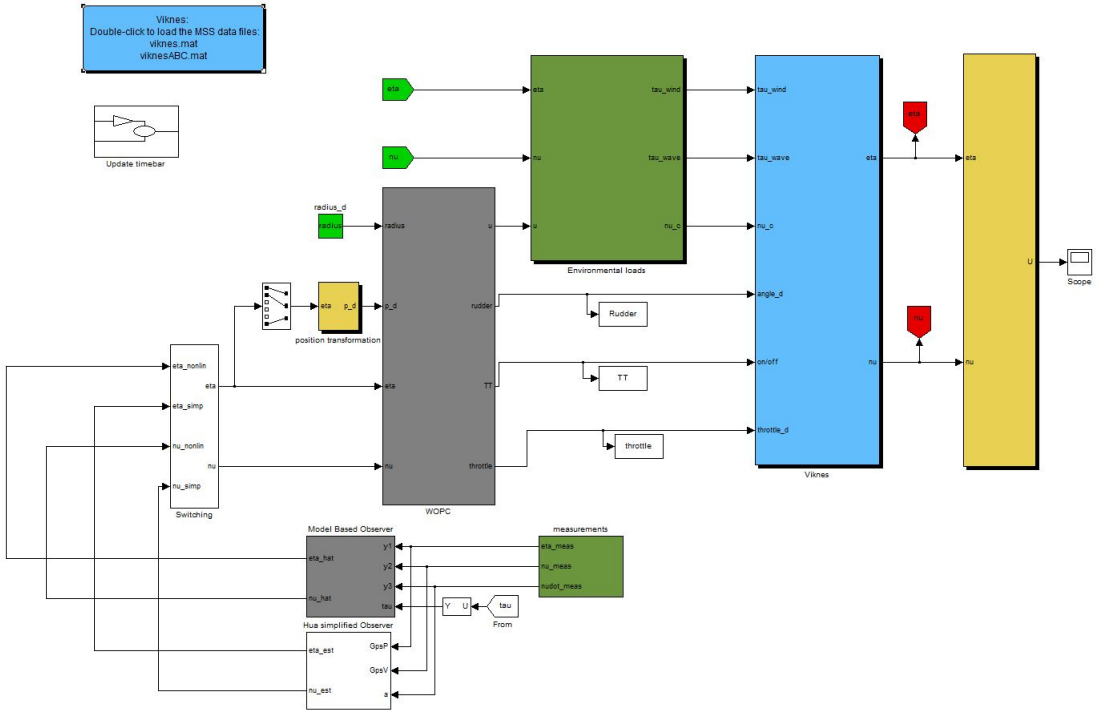

Figure 5.6: The Simulink block diagram of the whole Viknes 830 DP simulator.

The simulations were conducted with one observer at a time. Plots of measured and estimated states in addition to plots of the vessel trajectory and controller usage, were taken after each run. These plots are shown in this section along with a comparison of the two observeres, and a discussion of the results presented. The actual Simulink block diagram of the whole simulator can be seen i figure 5.6. In figure 5.7 the estimated North position of both observers are presented along with the measurement of the same state. It is clear that both observers removes the measurement noise satisfactory.

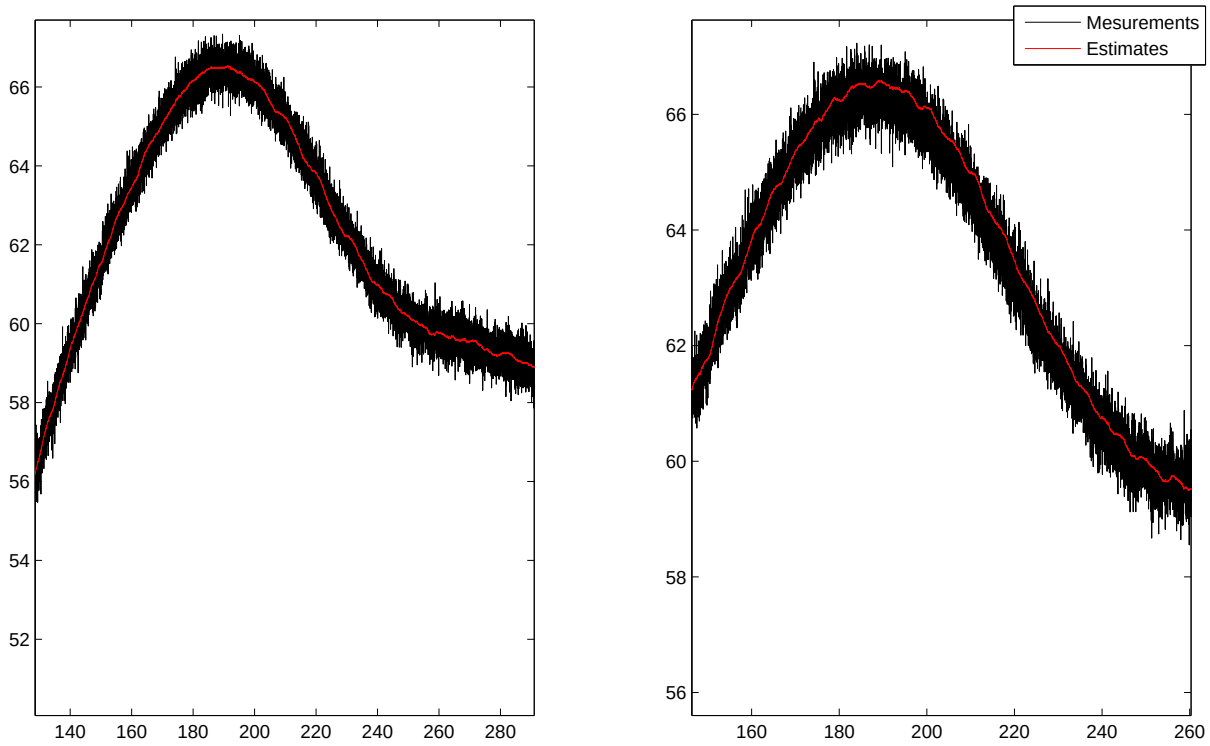

Figure 5.7: Position estimates compared to the actual measurement. The model based on the right and the simple on the left.

5.5.1 Simple Observer

Figures 5.8 and 5.9 shows how this observer managed to estimate the position, heading and velocity of the vessel. As can be seen, the estimates are smoother than the perfect measurements and there are less fluctuations. This implies that the WF motion of the waves was filtered out, and only the LF motion was allowed back in to the controller.

Unfortunately a small phase lag is evident, especially in the heading estimates. This is not surprising due to the wave filtering that is being done on the measurements before they enter the observer. The phase lag causes the heading to oscillate, although with a relatively small amplitude, this could cause excessive actuator usage and abrasion. Because of this phase lag, it is somewhat surprising that the vessel finds the desired position without any major deviations and with a relatively smooth trajectory, as can be seen in figure 5.10.

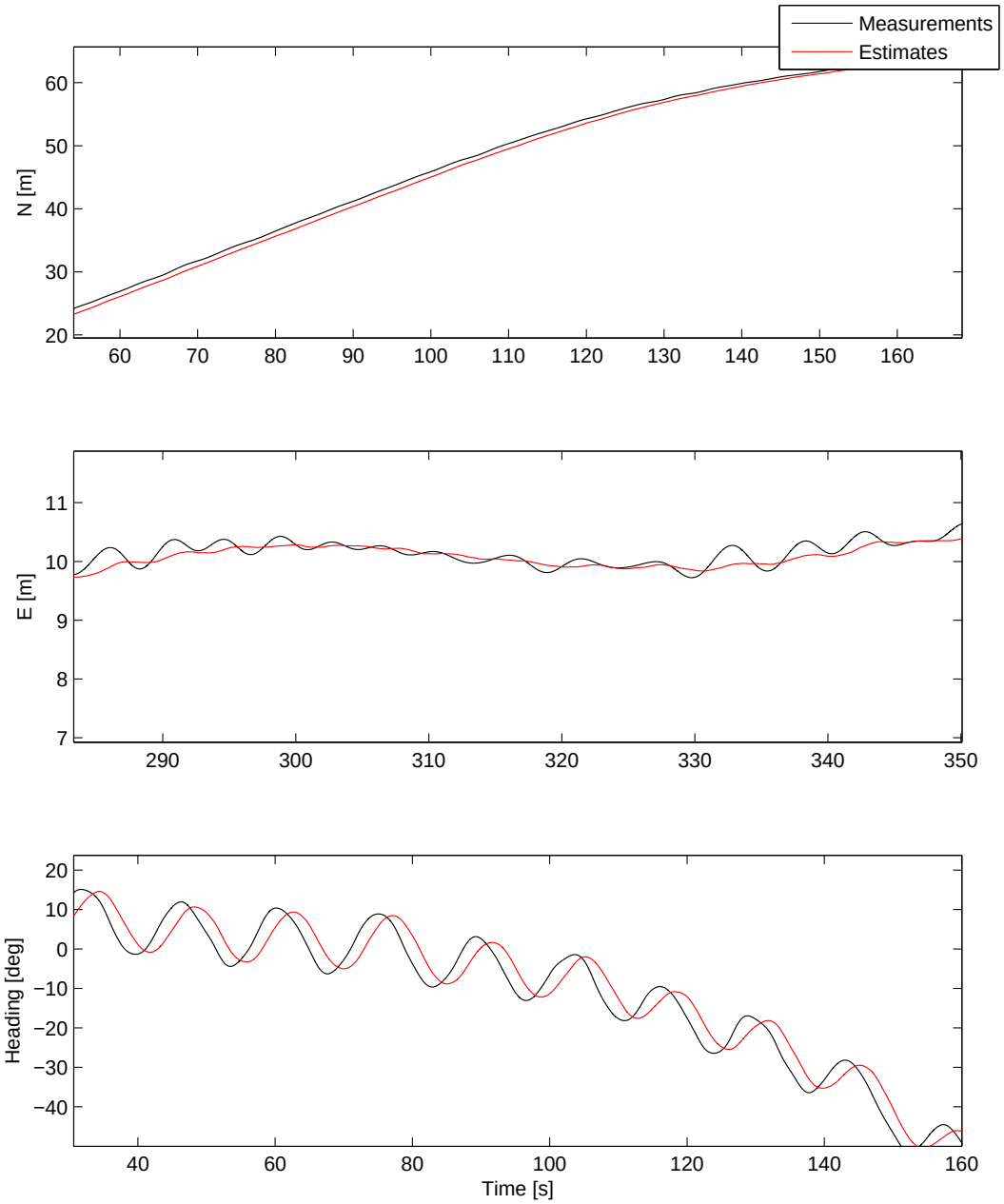

Figure 5.8: The position and heading estimates along with the perfect state measurements in the first scenario.

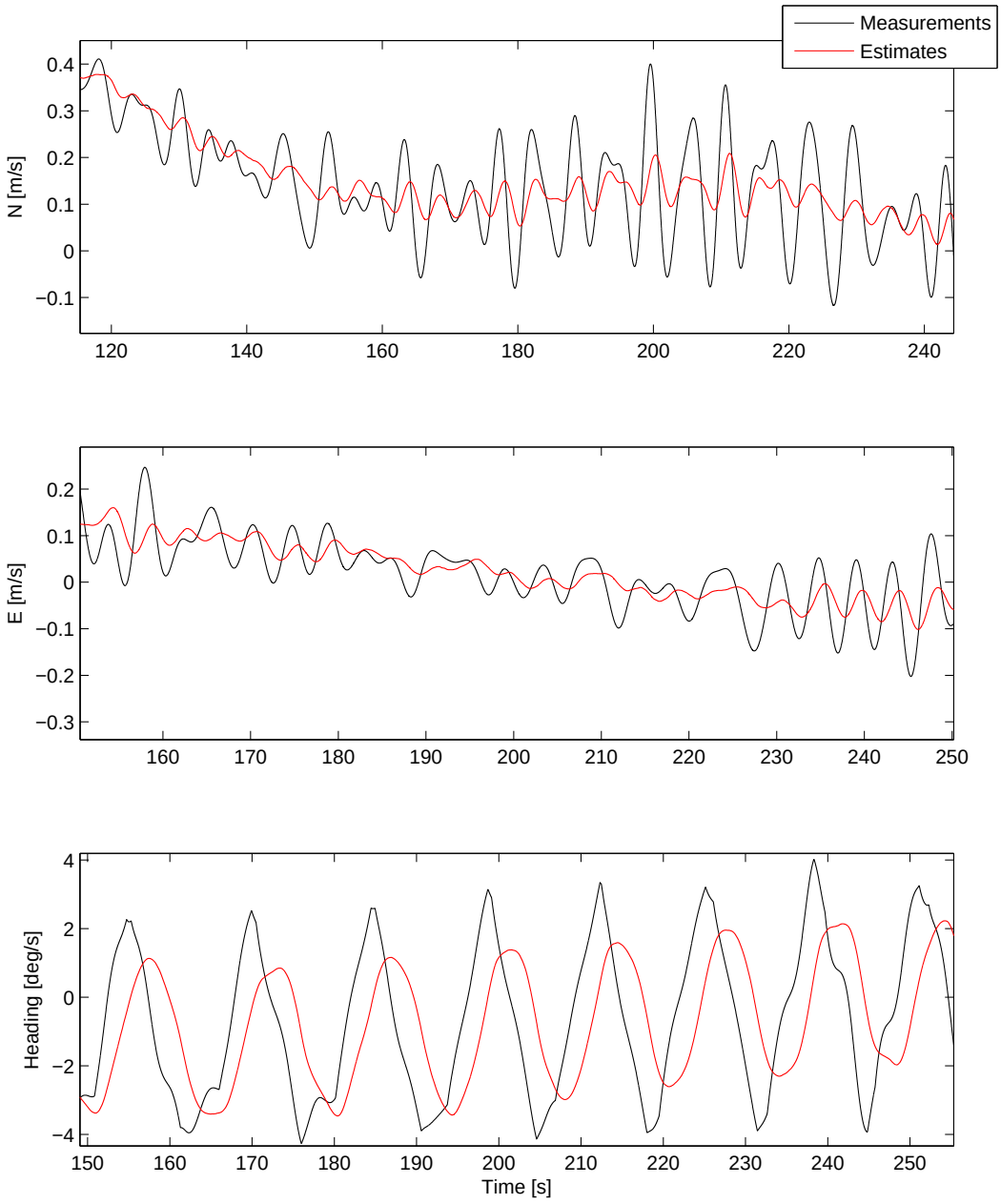

Figure 5.9: The velocity estimates in the first scenario.

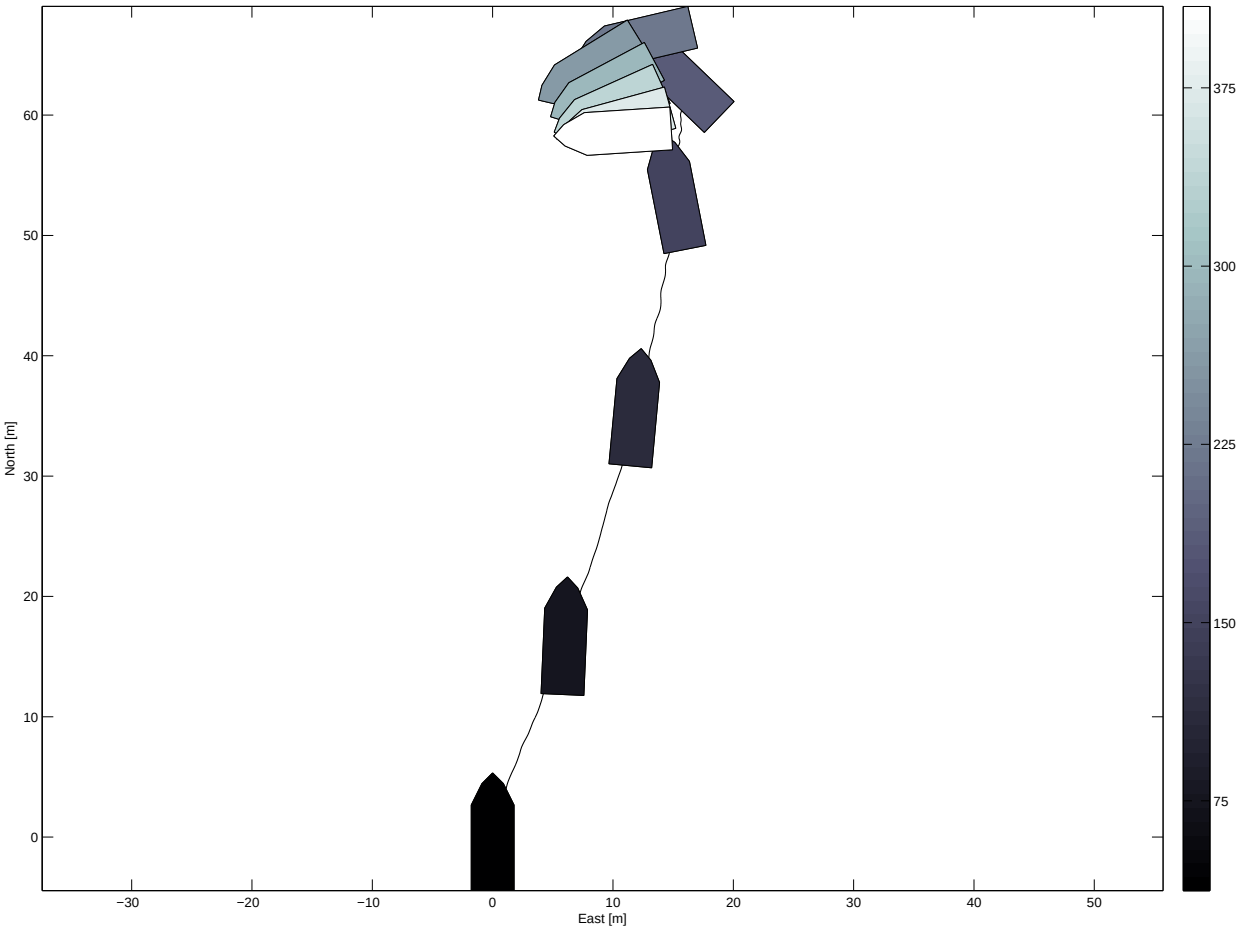

Figure 5.10: The USV traveling towards the desired position in calm sea.

In the first scenario the wind and waves were relatively easy to handle for the USV. However, in the second scenario both the wave height and wind speed increase significantly. I became evident that the initial tuning of the observer would not be good enough. The reason for this is most probably due to a frequency shift in the wave spectrum. It is reasonable to assume that larger waves, because of their size, have a lower peak frequency and a broader bandwidth. To deal with this, the notch in the notch filter had to be moved and widened. This means that the center frequency ω_i and the notch "width" δ_i had to be adjusted. By retuning the wave filter, the values that gave the the best estimates were

$$\begin{aligned} \omega_i &= 0.65 \\ \delta_i &= 7 \end{aligned}$$

The simulations runs can be seen in figure 5.11 and 5.12 .

Again the estimates are smoother than the measurements, illustrating that the wave filter works properly. Since the waves in this scenario is much bigger, the USV experience larger and more violent motions. Because of this, it is easier to see how much of the motion the wave filter removes, this is especially true in the East position and velocity plots. But also in these simulations a phase lag is present. This is of course not surprising after the first simulation, and it is with out a doubt a major drawback with this observer. Despite the oscillations occurring in the heading estimates due to the phase lag, figure 5.13 shows that the USV once again finds the desired position and the trajectory is relatively smooth.

The tuning of this observer was relatively easy. The wave filter for both observers were both tuned in the same way. The difference between the two is that for this observer the filter parameters are used directly in the wave filter, while for the model based observer filter the parameters are used in the observer gain matrices to create the notch- and low-pass filter effect.

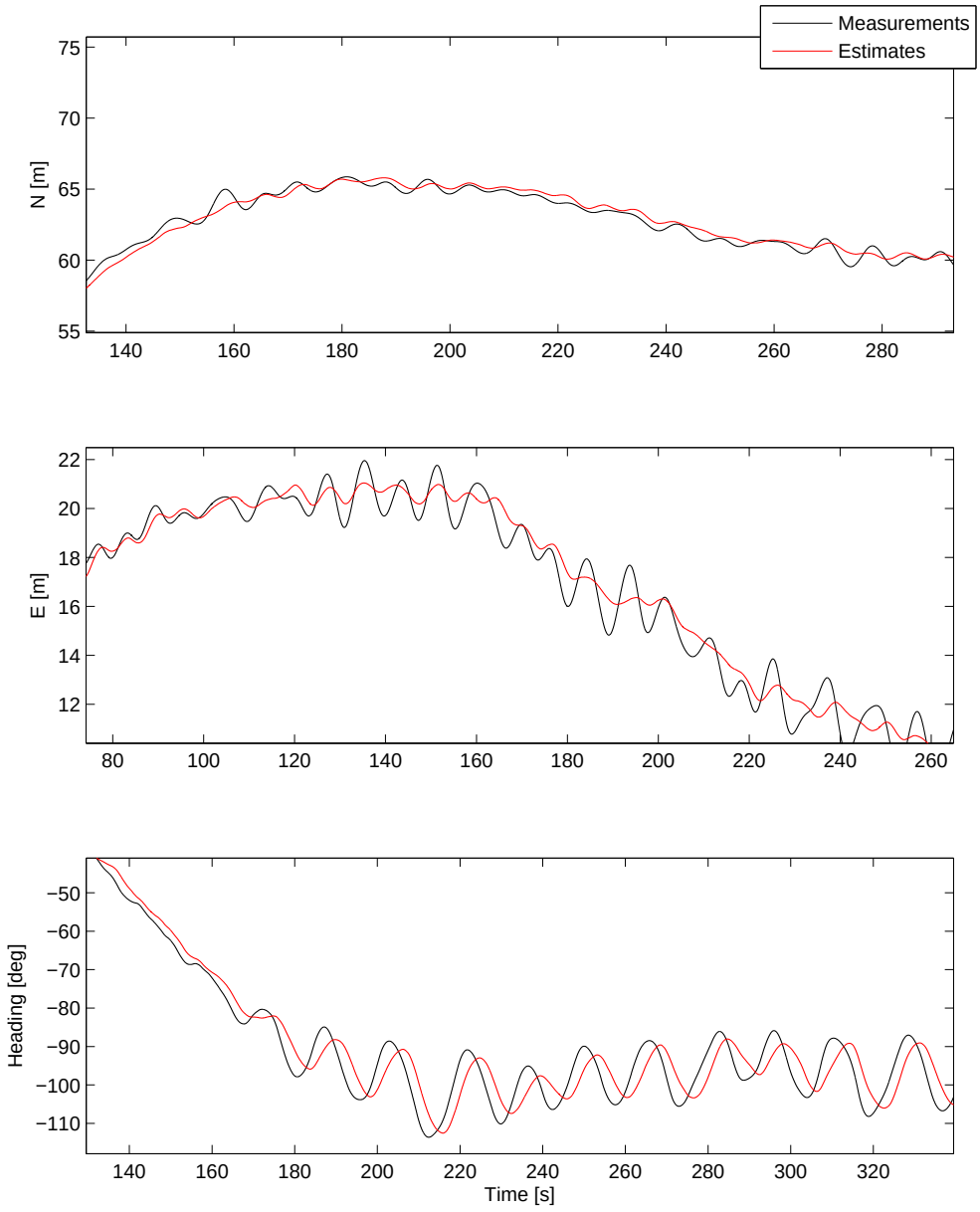

Figure 5.11: Position and heading estimates along with the perfect measurement in rough sea.

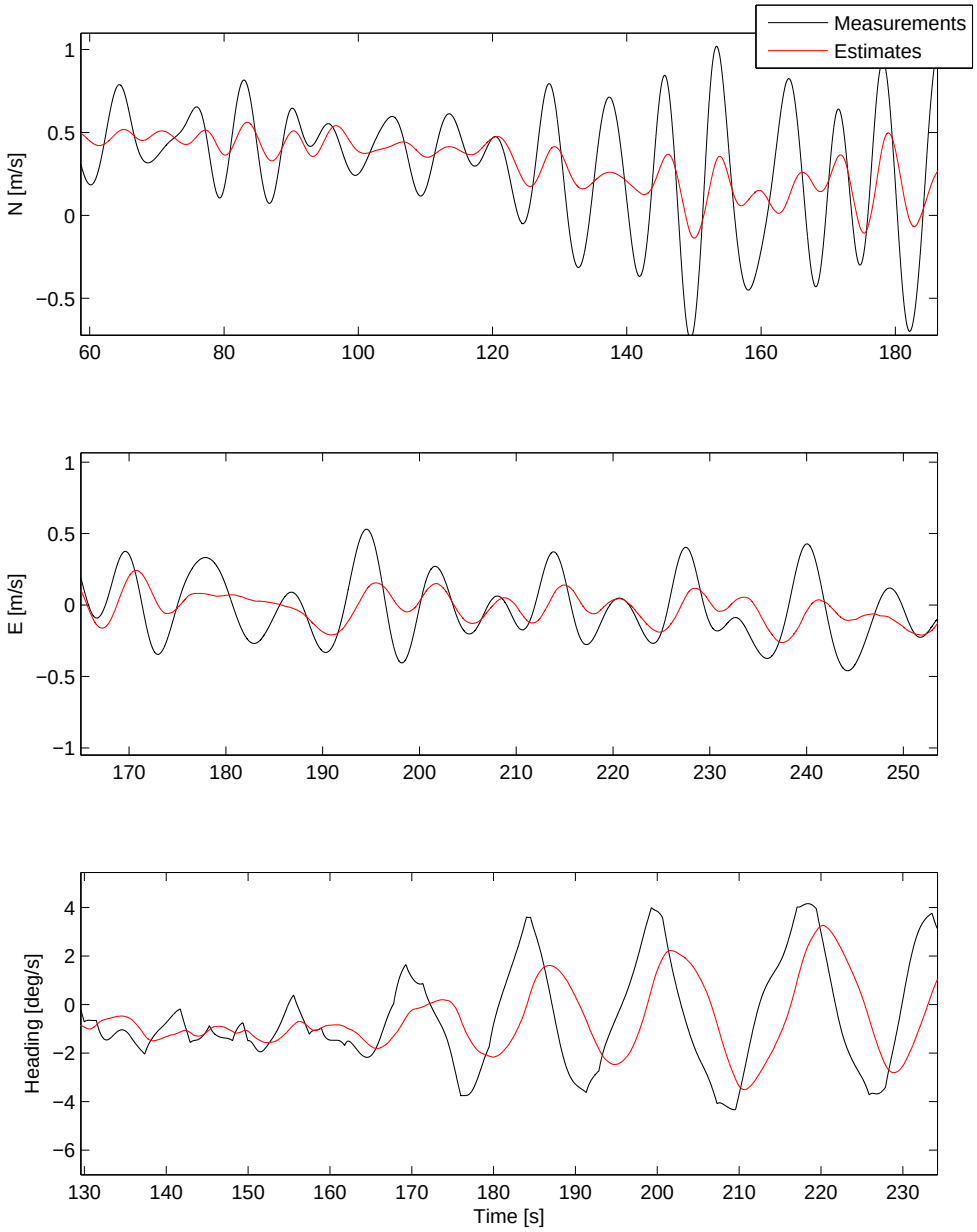

Figure 5.12: Velocity estimates along with the perfect measurement in rough sea. The phase lag is especially evident in the heading rate estimates.

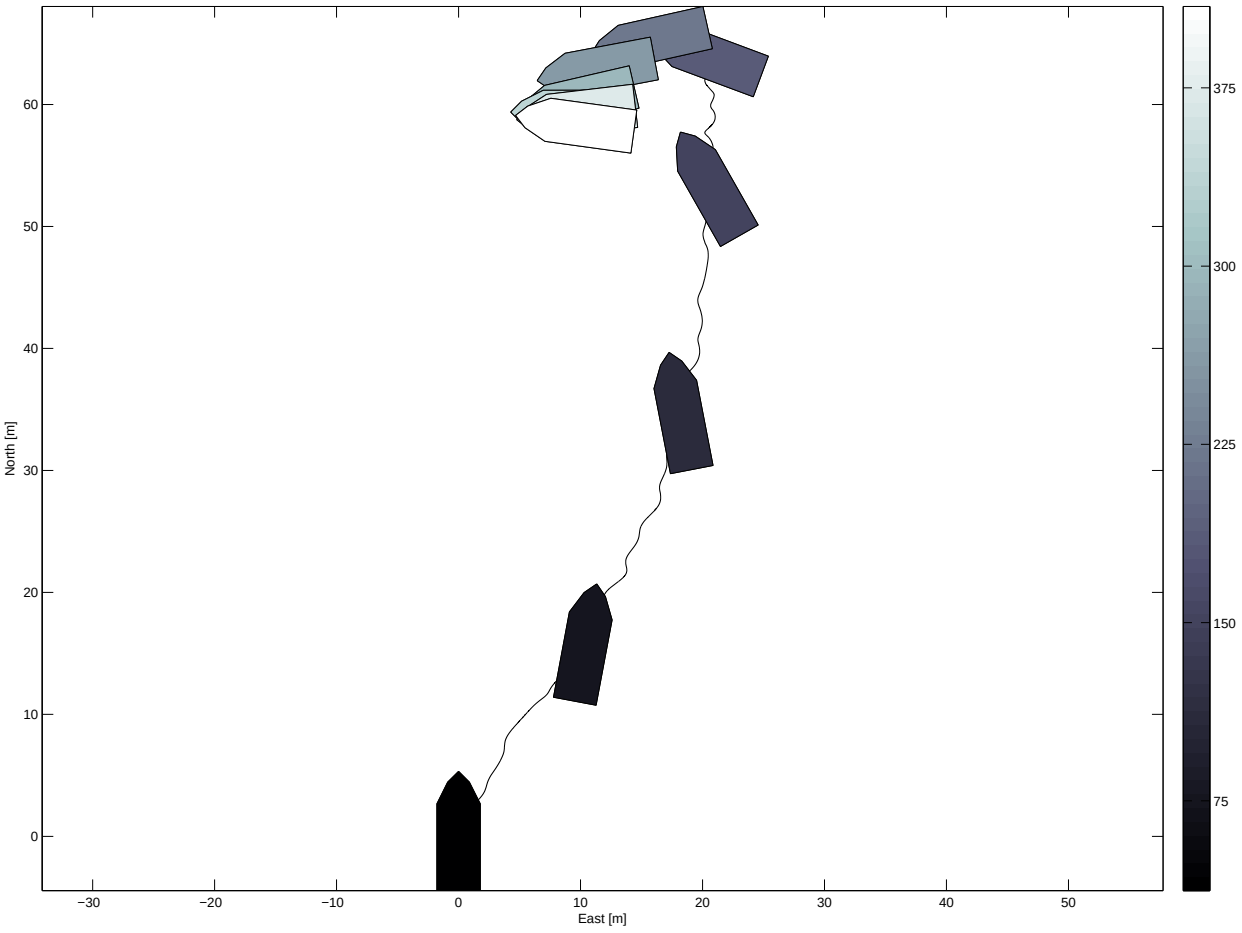

Figure 5.13: The USVs orientation and path towards the desired position is illustrated. Despite the rough sea, the USV manage to perform the task with success.

5.5.2 Model Based Observer

As mentioned, the measurement noise was reduced significantly by the model based observer. In figure 5.14 and 5.15, the estimated states of the USV in the calm sea state are shown. The measurements in the figures are the perfect measurements, they are not imposed by any noise. With this observer the state estimates are again smoother than the measurements, and it can be seen that most of the high-frequency motion is removed by the wave filter. Only the low-frequency motion is allowed back into the controller. However, the state estimates are not as smooth

as the ones seen in the previous section, and as figure 5.14 and 5.15 reveals, the noise filtering is not as good as with the model-free observer. With this observer, no phase lag is visible in the state measurements.

By following the tuning procedure, the process of finding suitable values for the different parameters were straight forward. The most difficult part was to find the right frequencies for the notch filtering of the measured signals. Fortunately, in Lindegaard (2003) the observer was tested, and by using the observer gain values found there as a starting point, only small adjustments had to be made in order for the observer to give satisfactory results. The wave filter in the previous section was also tuned with these values as a starting point. Figure 5.16 illustrates how the USV travels towards the desired position.

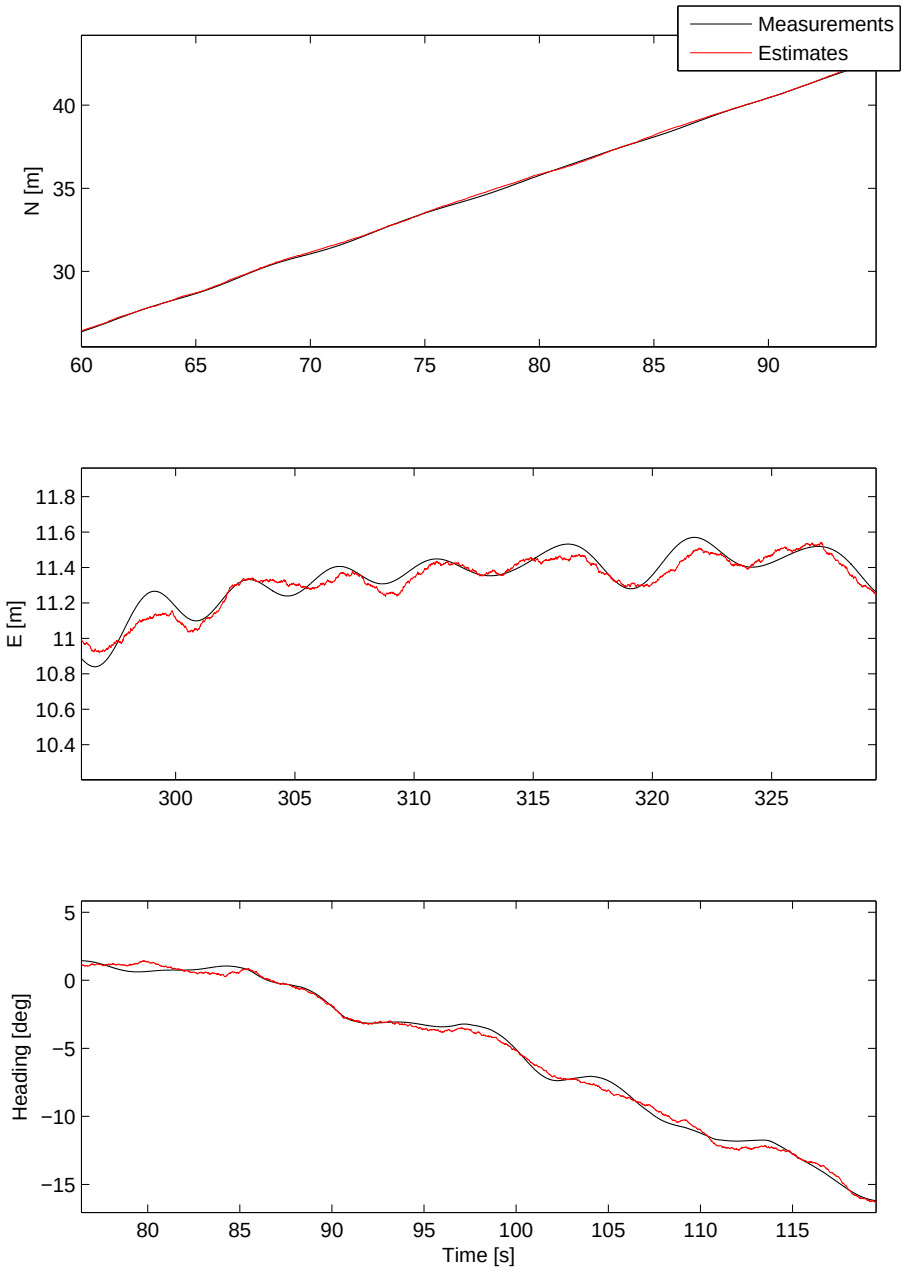

Figure 5.14: The Earth-fixed position and heading estimates generated by the model based observer in the calm sea state. The measurements are not imposed by any noise, and are therefore the perfect measurements.

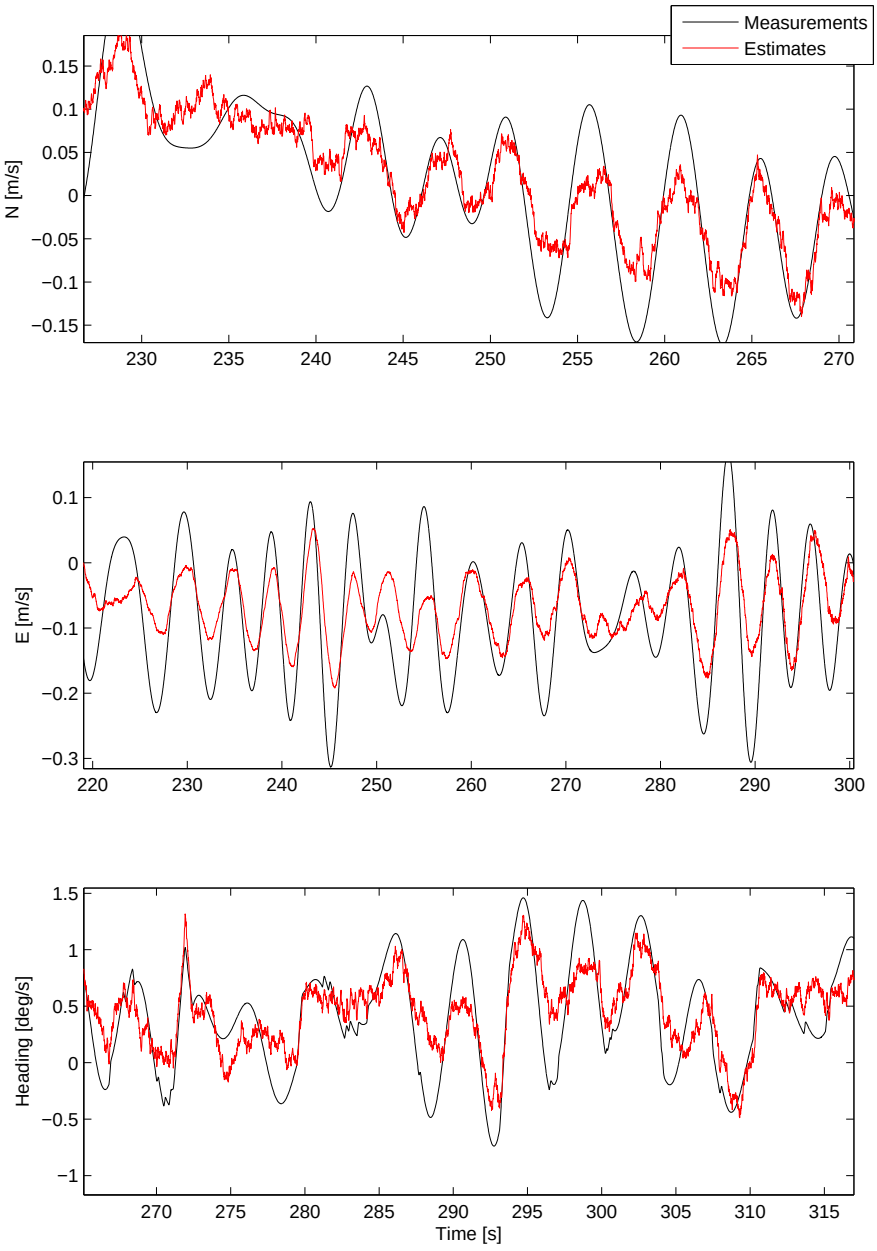

Figure 5.15: The estimated and measured (perfect) velocities in calm weather using the model based observer.

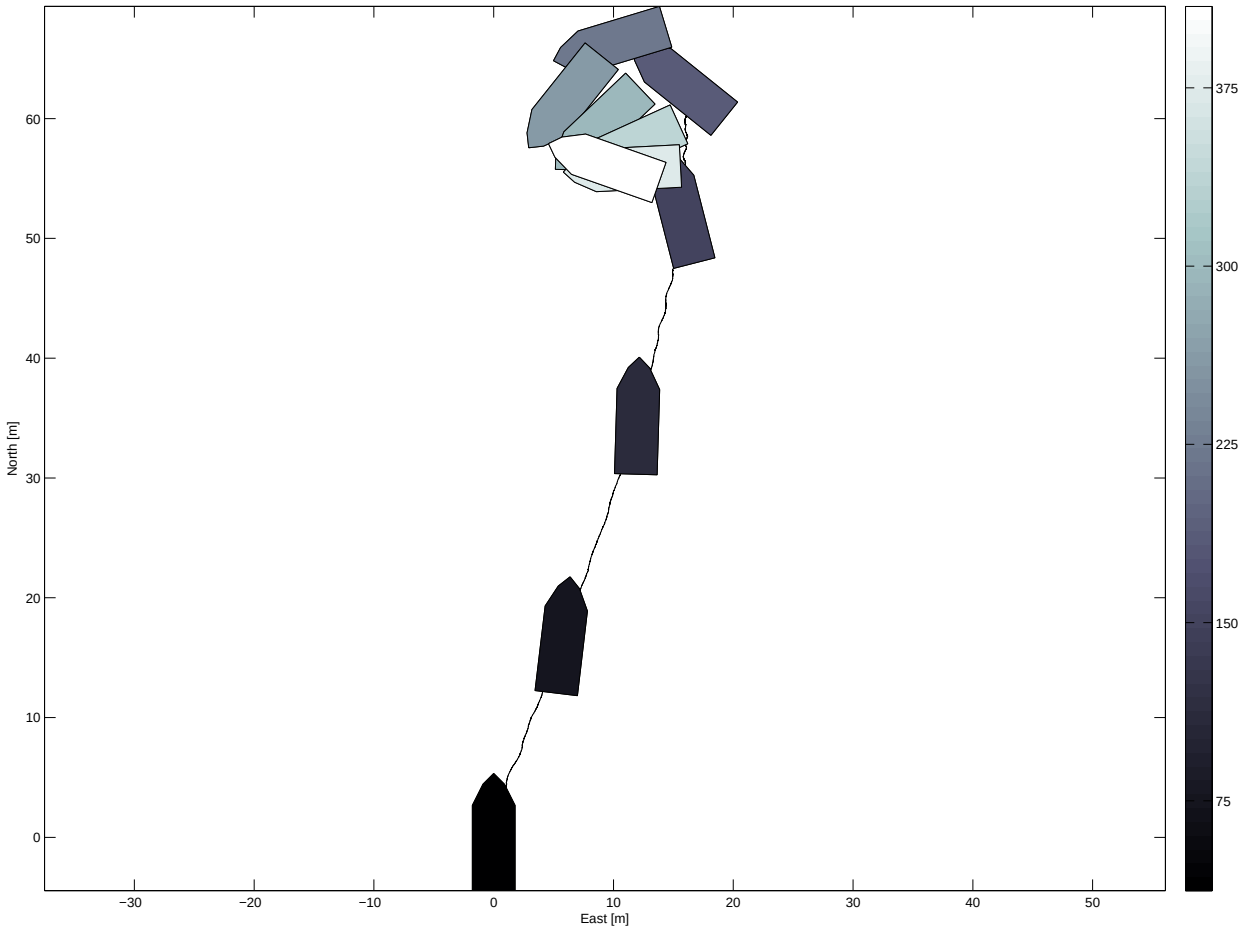

Figure 5.16: The USVs trajectory towards the desired position i calm weather conditions.

As with the first observer, the sea condition in the second scenario was more demanding than the first. The wave filter had to be adjusted for this observer too, meaning that the observer gains were altered. The center frequency ω_i and the notch width was adjusted in the same way as for the first observer. The new values was found to be

$$\begin{aligned} \omega_i &= 0.65 \\ \delta_i &= 7 \end{aligned}$$

The result can be seen in figure 5.17 and 5.18. Again, the estimated states have the same behavior as in the previous scenario.

Due to the more complex sea state some fluctuations in the estimates be accepted, still the performance of the observer is good. In figure 5.19 the USV and its trajectory towards the desired position is shown. The behavior of the vessel is satisfactory i.e. the heading is not fluctuating much. As for the first observer, the wave filtering becomes more evident in the second scenario. The trajectory is in this scenario is less smooth, but that is to be expected due to the weather condition. In all, the observer successfully managed to remove unwanted noise and the WF motion of the waves, and in addition the estimated states followed the measurements closely.

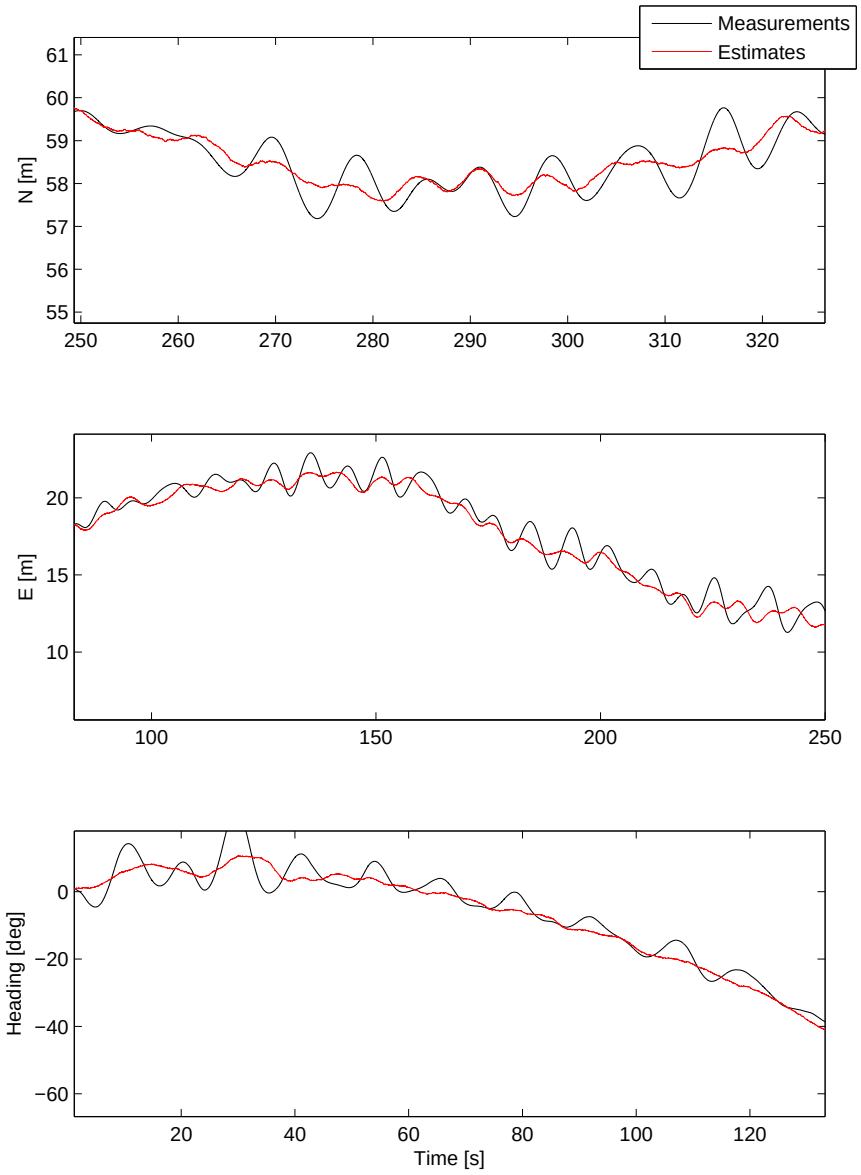

Figure 5.17: Estimated and (perfect) measurements of the position and heading in rough weather conditions.

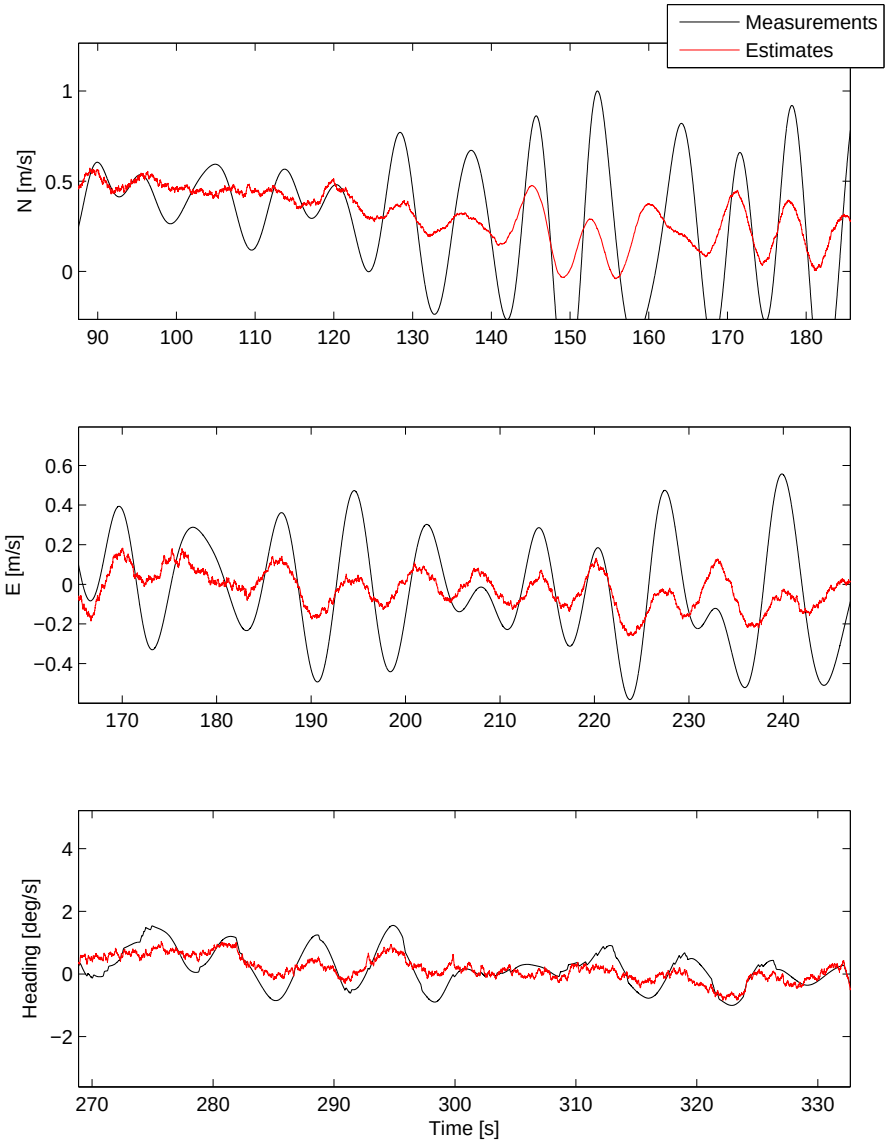

Figure 5.18: Estimated and measured velocities in rough sea.

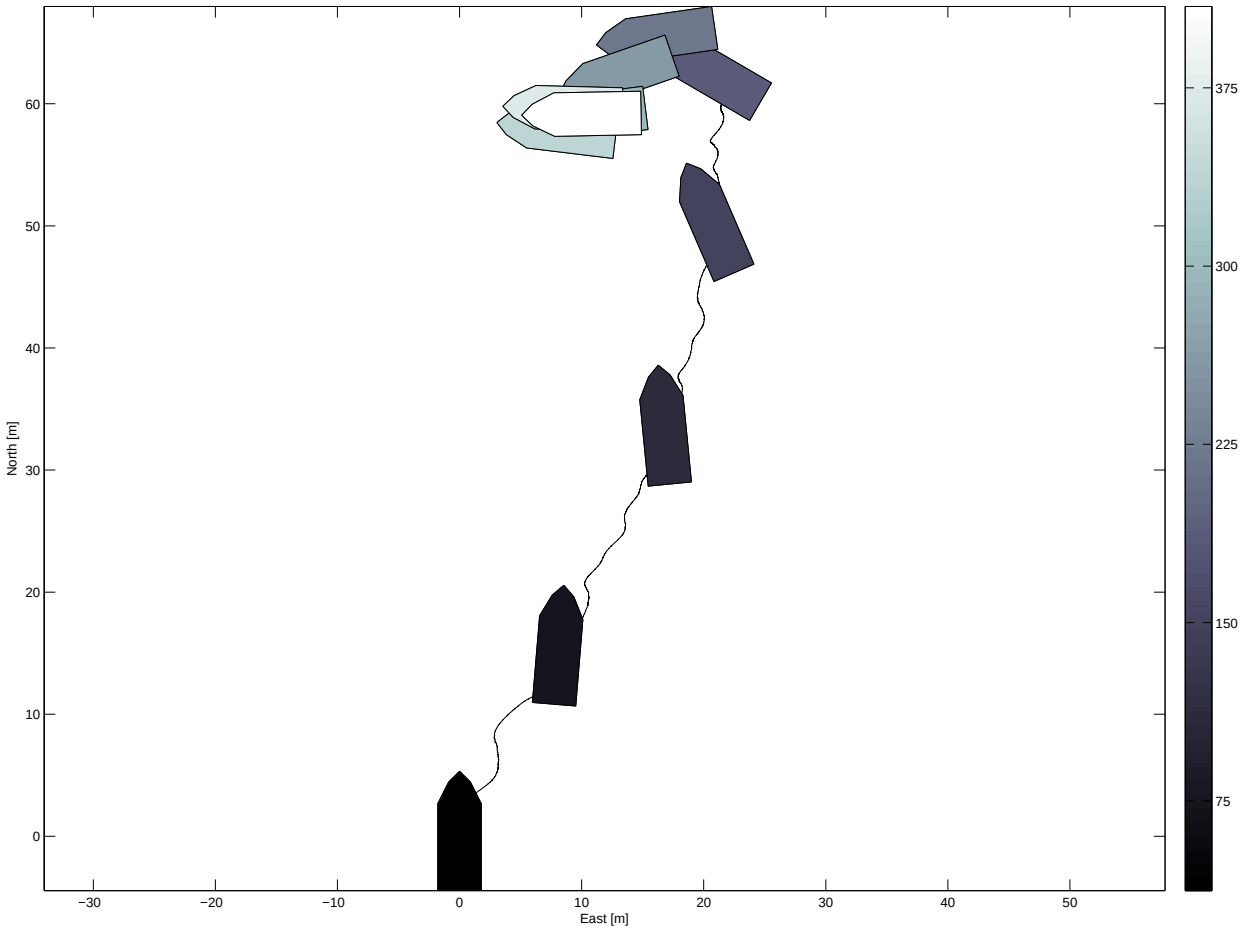

Figure 5.19: The USV and its trajectory towards the desired position.

5.6 Comparison and Discussion

By taking a look at the observers design and structure, some similarities and some differences are visible. Both observers makes use of measured acceleration, velocity, position and heading in order to generate state estimates. The first observer takes the measured acceleration as input, and with feedback from both GPS position, heading and velocity it generates smooth and accurate state estimates. When designing the observer, the wave filter were left out and instead the wave filtering is done outside the observer i.e. each measurement passes through the filter before

it enters the observer. Since the wave models is left out of the observer design, the observer structure is very simple, making the observer easy to understand and the observer gains relatively easy to find. A drawback with the design is that both the observer and the observer gains have to be tuned separately. Unfortunately the observer lacks bias estimation.

The second observer is based on a 3 DOF low-frequency model of the Viknes 830. In contrast with the first observer, this observer makes it optional if the measured velocity and acceleration should be used as feedback, while the position and heading are always used. This makes the observer more versatile and operator friendly. The observer also includes bias estimation. The wave models used are the same in both observers, the difference is that in this observer, the wave models are a part of the observer design. This, combined with the vessel model makes the observer structure and design very complex, and the observer gains are not as intuitive as in the first observer. In addition, the observer requires estimates of the actuator thrust forces as input which can be difficult to obtain.

Comparing the two observer's estimates some differences are evident. For the first and simplest observer a phase lag is visible in the plots. This phase lag is a result of how the wave filtering is done. Since the measurements passes through a filter before entering the observer, it is hard, if not impossible, to avoid the phase lag. The phase lag severely degrades the estimates, and because of the lag the heading starts to oscillate. Although the amplitude of the oscillations is relatively small, it has a significant influence on actuator usage and performance of the DP system, this will be addressed later in the text. The model based observer has far better results. The state estimates are not as smooth as with the simple observer, the estimates are marginally more noisy, but there is no phase lag. As mentioned, the wave models used are the same in both observers, this indicates that by including the wave model in the observer design might help to remove or reduce the phase lag, in addition an observer based on a vessel model should be better suited to keep up with and predict the states of the vessel.

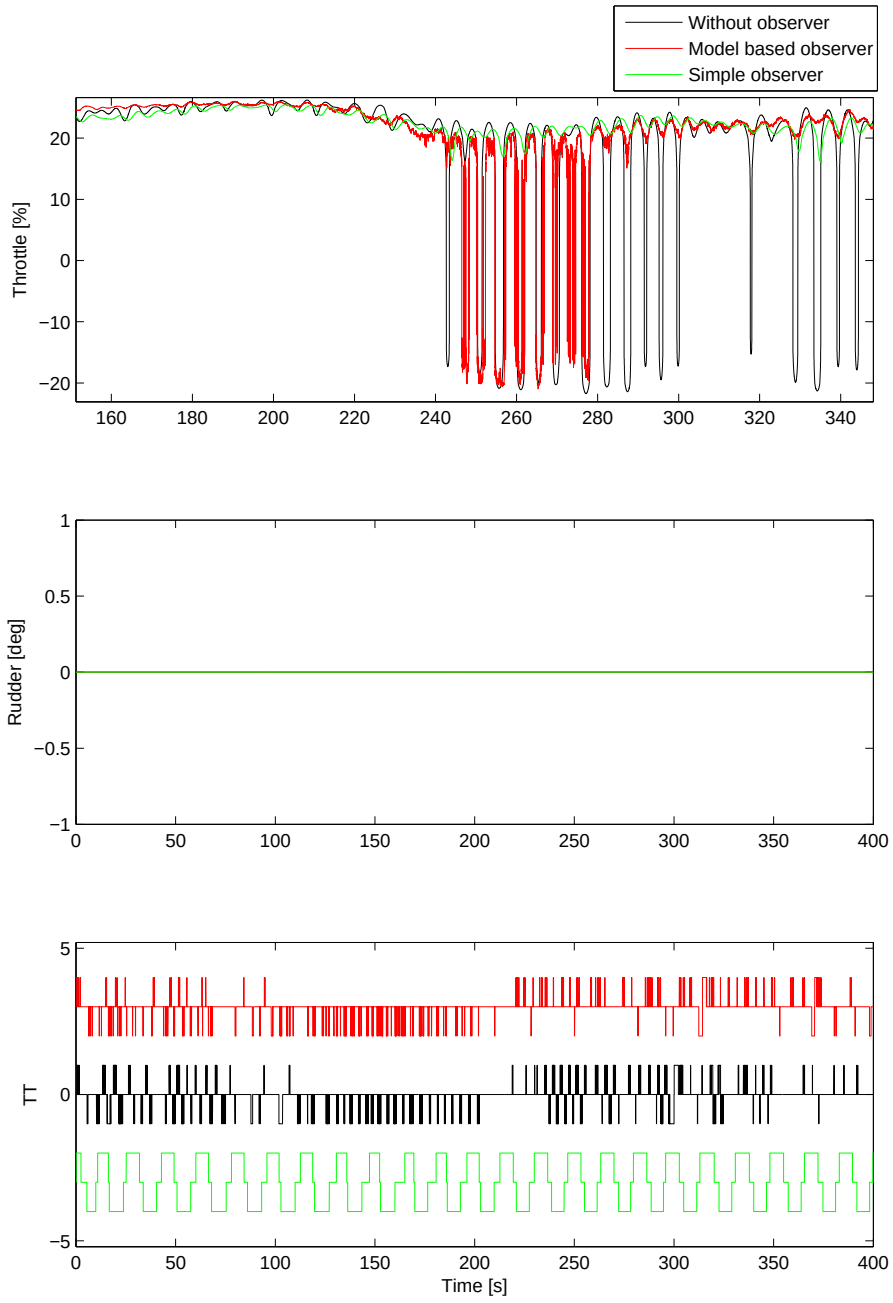

Figure 5.20: The controller set-points illustrates how much the controller have to work in order to find and keep the desired position. The tunnel thruster usage is scaled to fit the plot.

Figure 5.20 shows the controller set-points in the first scenario. Each plot contains three different runs, one without any of the observers, and one run for each of the proposed observers. For the first 240 seconds the throttle is fairly similar for both observers, but after this the throttle controller behavior becomes different. The first observer removes all throttle spikes compared to the reference run, while the model based observer removes the majority of the spikes occurring in the reference run, but not as good as the simple one. In all three runs the estimated water speed across the rudder does not exceed 1 [m/s], thus the rudder is never used. The tunnel thruster set-points are interesting. It shows that the model based observer reduces the tunnel thruster usage by approximately 20 %. The simple observer however, significantly increases the tunnel thruster controller usage. This might explain the significant reduction in throttle spikes when using this observer. The tunnel thruster set-points generated when using the first observer oscillates throughout the whole run. Such a behavior is no good and could lead to abrasion and damage of the actuator. According to Kjerstad (2010), the continuous run-time is constrained to 25 [s]. With the simple observer the tunnel thruster set-points oscillates between opposite bursts which lasts approximately 7 seconds, with very little rest in between.

In a reference run without using any of the observers in the feedback loop, it took the USV 297.1 [s] to converge to the desired position. It is often a trade off between fast convergence and actuator usage in DP operations, the most desirable result is of course to reduce both. With the model based observer the USV was able to get to the position set-point in 277.4 [s], reducing the convergence time by approximately 7 %. This is remarkable considering it also reduced the actuator usage as well. By switching observers, the time it took to obtain the desired position was 337.4 [s], which is significantly longer than the model based observer and compared to the reference run it is an increase of approximately 13 %. Figure 5.21 shows USV trajectory with each of the observers and the reference run.

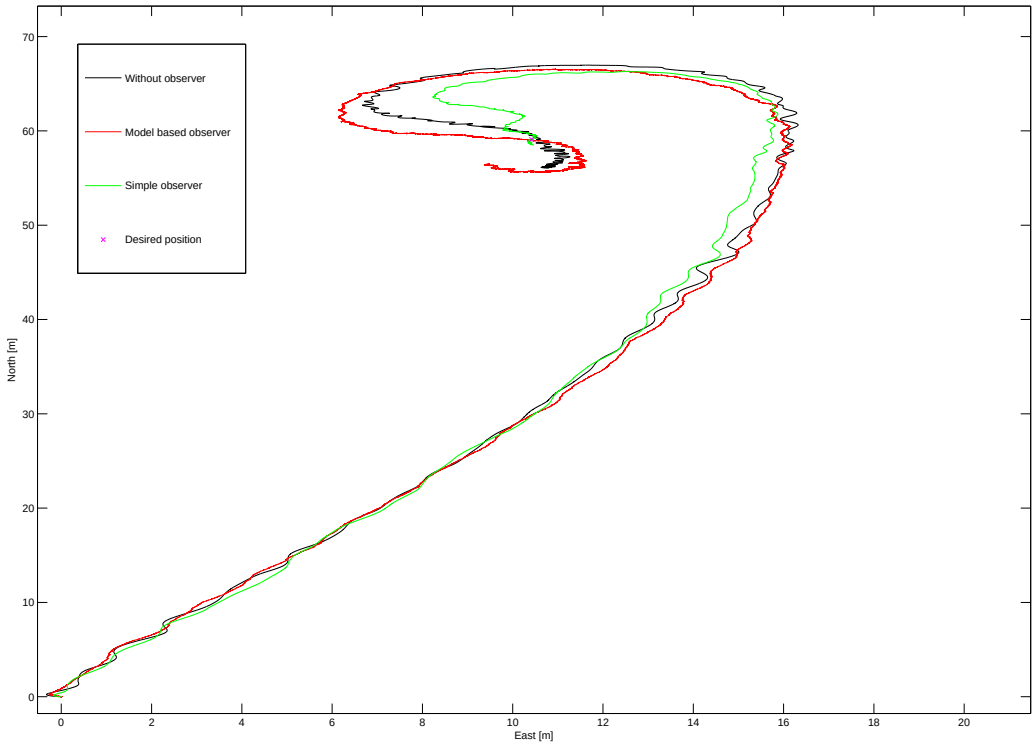

Figure 5.21: The vessel trajectories for the comparison runs.

Both observers improves the trajectory compared to the reference run. Some of the sideways movement is removed making the trajectories smoother. The USV have different approaches to the desired position depending on which observer being used. With the model based observer the trajectory has the same shape as in the reference run, but with the simple observer, the trajectory seems a bit more cautious and since the convergence time increased, this is a valid assumption.

The most probable reason for the first observer's bad performance is the phase lag. It has a significant effect on the state estimates and on the performance of the DP system. As mentioned, the phase lag is not unexpected due to the way the wave filtering is done, unfortunately the it generates a delay in the estimates causing the heading to oscillate. An experiment was conducted where the measurements did not pass through a wave filter before they entered the simple observer. The result can be seen in figure 5.22. The estimates are now much better, although the WF motion is not removed from the measurements in this case. This is indicates how the current wave filter implementation imposes a phase lag on the estimates.

A solution to this problem could be to integrate the wave models in the observer design. This would make the observer structure more complex, but it could reduce the phase lag.

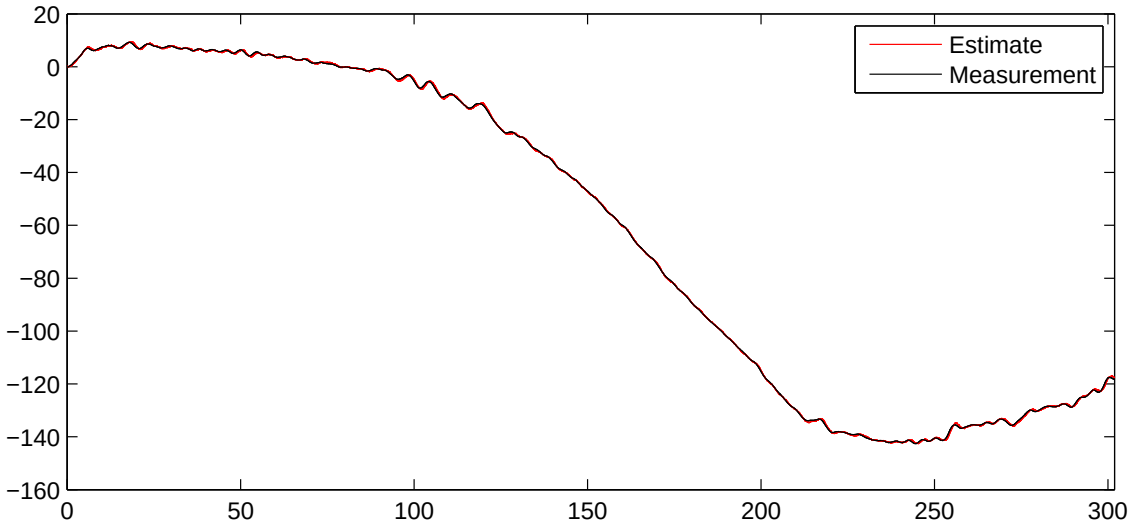

Figure 5.22: Estimated and measured heading without wave filter, using the simple observer

The model based observer has this feature. The wave filter is a part of the observer design and in addition the observer is based on a model of the Viknes 830. This observer gives by far the best performance of the two, and it improves the DP performance significantly compared to not using an observer. It allows the operator to choose what measurements he wish to utilize, and the tuning process consists mainly of placing the wave filter correctly. The drawback is the need for a detailed vessel model which is not always easy to obtain. It also require measurements or estimates of the actuator thrust forces. The results however, suggests that this observer could be tested on the real USV. The first observer does have potential, and if the phase lag could be avoided it would probably give the best estimates, but for it current design, it might not be wise to test the observer at sea.

Chapter 6

Conclusion and Further Work

In this thesis two observers have been proposed. The goal was to investigate what benefits that could be achieved by removing the high-frequency wave motion from the measurements, and also to explore the use of acceleration feedback to improve state estimation. Both observers utilized the measured acceleration in the state estimation, and i both cases wave filtering was implemented. The observers were to be tested together with a DP system developed in Kjerstad (2010) in order to improve the performance of the DP system. The observeres were tested in a Matlab/Simulink simulator and the results was evaluated.

For conventional DP systems on large vessels it is common to remove the WF motion of the waves from the measurements, while a common assumption for small vessels is that this motion has to enter the feedback loop in order for the vessel to be able to maintain a position. The results presented in this thesis shows that this is not necessarily the case.

The first observer, a simplified attitude observer, used the measured acceleration as input and the wave filtering was done before the measurements entered the observer. The observer was tested in two scenarios in order to investigate its performance. The noise filtering was excellent in both simulations, and the state estimates generated had the same shape as the perfect measurements i.e. measurements without any noise. Unfortunately, the wave filter imposed a phase lag on the state estimates. This caused the heading and the tunnel thruster control signal to oscillate, a situation that could be demanding for the vessel to handle, and that could lead to excessive wear and tear of the actuators. The result was that both controller usage and convergence time was significantly increased, indicating that the observer was unsuited as a state estimator in its current configuration and design. However, it performed excellently when the wave filter was removed, and could possibly be improved by integrating the wave filter differently.

The second observer presented was more complex in design and structure. The

whole observer was based on a 3 DOF LF model of the Viknes 830 with the actuator thrust forces as input. In addition, the wave models were integrated in the observer design. This made the tuning process more difficult and less intuitive. Again the measurement noise was removed, and the state estimates delivered by this observer in the simulations proved to reduce both convergence time and controller usage, which is an ideal result. The estimates were marginally more noisy than with the first observer, but by reducing both convergence time and controller usage, it did give the best simulation results of the two.

The simulation results for the model based observer showed that the performance of the DP system was improved when the WF motion of the waves was removed. Unfortunately, because of the phase lag, the simulations with the model-free observer was not able to verify this. This result should however be subject to further investigation, and there are also other aspects that should be considered in the future:

- Sea trials. Sea trials were originally planned to be conducted as a part of this thesis, but due to unforeseen hardware malfunction in the Viknes 830 this could not be carried out.
- Improving the model-free observer. A phase lag was introduced by the wave filter. A different wave filtering scheme should be tested in order to remove or decrease the lag.
- Thrust estimation. The thrust estimation needed for the model based observer could be improved and verified by tests.
- C code implementation of the observers. Better real-time capabilities could be achieved by implmenting the observers in the on-board computer.
- New tunnel thruster. The current tunnel thruster has only an on-off setting. By fitting a proportional thruster and changing the tunnel thruster model in the simulator, better performance could be achieved.

Appendix A

Furuno SC-50 Data Sheet

SPECIFICATIONS OF SC-110

1. Accuracy

Heading:	±0.6° (95 % static accuracy) (IMO THD MSC.116(73) static accuracy: ±1.0° x secant Lat.)
GPS:	10 m (95 %)
DGPS:	5 m (95 %)
2. Follow-up	25°/s rate-of-turn
3. Settling time	4 min
4. Interface	
Number of ports	
10 ports*	5 ports in AD-10 or 10 ports in IEC 61162-1/-2
* Number of ports is changed by system configuration.	
1 port	AD-10 only
Serial data sentence	
25/100/200 ms, 1s data rate:	HDT, HDM(Heading), Patt(Pitch, Roll and Yaw), ROT(Rate of turn)
1/2 s data rate:	VHW(Heading), VTG, VBW(SOG), GGA, GLL, GNS(L/L), ZDA(UTC), GSA, GSV
Log Output	1 port: 200/400 p/nm (closure)
Alarm Output	1 port: Alarm signal (closure signal)
Heading Input	1 port: Backup Heading (AD-10/IEC 61162-1/-2) HDT, HDG, HDM, VBW, VHW, VLW
DGPS Input	1 port: RTCM SC-104 format
5. Receiver Type	Twelve discrete channels. C/A code, all-in-view
6. Receive Freq	L1 (1575.42 MHz)
7. Display Unit	4.5" diagonal 95 (W) x 60 (H)mm, 120 x 64 pixels
8. Display Mode	Steering, Nav Data, Set and Drift, Compass Rose, ROT, Heading
POWER SUPPLY	12-24 VDC, 15 W

ENVIRONMENTAL

IEC 60945 for EMC, Vibration, Temperature

EQUIPMENT LIST

Standard

1. Display Unit SC-502	1 unit
2. Antenna Unit with 15 m cable SC-1203F	1 unit
3. Processor Unit SC-1101	1 unit
4. Standard Spare Parts, Installation Materials	1 set

Optional

1. Antenna Cable, 15 m 20S0336-1, 30 m CP20-01700, 50 m CP20-01710
2. Flush Mount Kit S type CP20-17, F type CP20-29
3. Repeater Interface for synchro or step by step

Display Unit 0.6 kg 1.3 lb

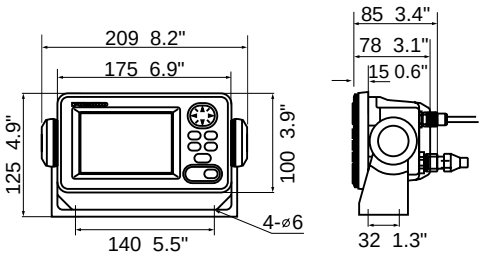

Processor Unit 3.6 kg 7.9 lb

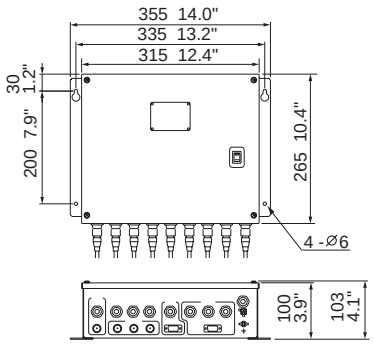

Antenna Unit 6.8 kg 15.0 lb

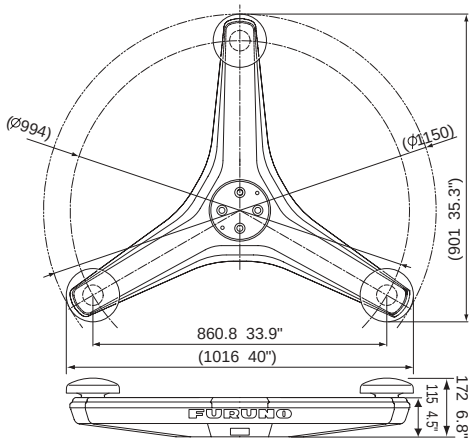

SPECIFICATIONS SUBJECT TO CHANGE WITHOUT NOTICE

02085Y Printed in Japan

FURUNO U.S.A., INC.
Camas, Washington, U.S.A.
Phone: +1 360-834-9300 Telefax: +1 360-834-9400

FURUNO (UK) LIMITED
Denmead, Hampshire, U.K.
Phone: +44 2392-230303 Telefax: +44 2392-230101

FURUNO FRANCE S.A.
Bordeaux-Mérignac, France
Phone: +33 5 56 13 48 00 Telefax: +33 5 56 13 48 01

FURUNO ESPANA S.A.
Madrid, Spain
Phone: +34 91-725-90-88 Telefax: +34 91-725-98-97

FURUNO DANMARK AS
Hvidovre, Denmark
Phone: +45 36 77 45 00 Telefax: +45 36 77 45 01

FURUNO NORGE A/S
Ålesund, Norway
Phone: +47 70 102950 Telefax: +47 70 127021

FURUNO SVERIGE AB
Västra Frölunda, Sweden
Phone: +46 31-7098940 Telefax: +46 31-497093

FURUNO SUOMI OY
Helsinki, Finland
Phone: +358 9 341 7570 Telefax: +358 9 341 75716

Appendix B

Microstrain 3DM-GX1 Data Sheet

3DM-GX1® Gyro Enhanced Orientation Sensor

3DM-GX1® utilizes the triaxial gyros to track dynamic orientation and the triaxial DC accelerometers along with the triaxial magnetometers to track static orientation. The embedded microprocessor contains a unique programmable filter algorithm, which blends these static & dynamic responses in real time.

This provides a fast response in the face of vibration and rapid movement while eliminating drift. The stabilized output is provided in an easy-to-use digital format. Analog output voltages proportional to the Euler angles can be ordered as an option.

Full temperature compensation is provided for all nine orthogonal sensors to insure performance over a wide operating temperature range.

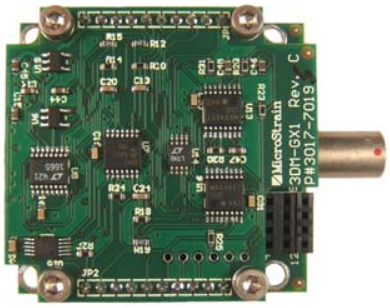

3DM-GX1's® small size is ideal for OEM applications.

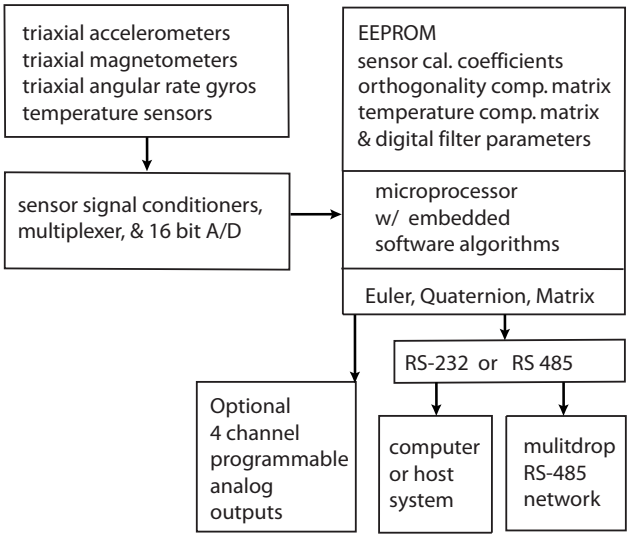

Specifications

Orientation range (pitch, roll, yaw)	360° all axes (orientation matrix, quaternion) ± 90°, ± 180°,± 180° (Euler angles)
Sensor range	gyros: ± 300°/sec FS accelerometers: ± 5 g FS magnetometers: ± 1.2 Gauss FS
A/D resolution	16 bits
Accelerometer nonlinearity Accelerometer bias stability*	0.2% 0.010 g
Gyro nonlinearity Gyro bias stability*	0.2% 0.7°/sec
Magnetometer nonlinearity Magnetometer bias stability*	0.4% 0.010 Gauss
Orientation resolution	<0.1° minimum
Repeatability	0.20°
Accuracy	± 0.5° typical for static test conditions ± 2.0° typical for dynamic (cyclic) test conditions & for arbitrary orientation angles
Output modes	matrix, quaternion, Euler angles, & nine scaled sensors with temperature
Digital outputs	serial RS-232 & RS-485 optional with software programming
Analog output option	4 channel, 0–5 volts full scale programmable analog outputs
Digital output rates	100 Hz for Euler, Matrix, Quaternion 350 Hz for nine orthogonal sensors only
Serial data rate	19.2/38.4/115.2 kbaud, software programmable
Supply voltage	5.2 VDC minimum, 12 VDC maximum
Supply current	65 mA
Connectors	one keyed LEMO, two for RS-485 option
Operating temp.	-40 to +70°C with enclosure -40 to +85°C without enclosure
Enclosure (w/tabs)	64 mm x 90 mm x 25 mm
Weight (grams)	75 grams with enclosure, 30 grams without enclosure
Shock limit	1000 g (unpowered), 500g (powered)

*Accuracy and stability specifications obtained over operating temperatures of -40 to 70°C with known sine and step inputs, including angular rates of ± 300° per second.

For additional information, please refer to "3DM-GX1 - Detailed Specifications", available online at www.microstrain.com.

MicroStrain®

MicroStrain Inc.
310 Hurricane Lane, Unit 4
Williston, VT 05495 USA
www.microstrain.com

ph: 800-449-3878
fax : 802-863-4093
sales@microstrain.com

Patent Pending

Bibliography

O. K. Kjerstad, Weather-Optimal Positioning Control for Underactuated USVs, Master's thesis, Norwegian University of Technology and Science, 2010.

M. Breivik, Nonlinear Maneuvering Control of Underactuated Ships, Master's thesis, Norwegian Unversity of Technology and Science, 2003.

T. I. Fossen, J. P. Strand, Passive Nonlinear Observer Design for Ships Using Lyapunov Methods: Full-Scale Experimentswith a Supply Vessel, Automatica .

J. Holvik, Basics of Dynamic Positioning, in: Basics of DP, 1, 1998.

B. Vik, Integrated Satellite and Inertial Navigation Systems, 2010.

J. G. Balchen, N. A. Jenssen, E. Mathisen, S. Sælid, A Dynamic Positioning System Based on Kalman Filtering and Optimal Control, Modeling, Identification and Control 1 (3) (1980) 135–163.

K. P. W. Lindegaard, Acceleration feedback in Dynamic Positioning, Ph.D. thesis, Norwegian University of Science and Technology, 2003.

T. I. Fossen, Marine Craft Hydrodynamics and Motion Control, Wiley, 1 edn., ISBN 978-1-119-99149-6, 2011.

M.-D. Hua, Attitude estimation for accelerated vehicles using GPS/INS measurements, Control Engineering Practice 18 (7) (2010) 723 – 732, ISSN 0967-0661, URL `http://www.sciencedirect.com/science/article/pii/S0967066110000249`, special Issue on Aerial Robotics.

Marinecontrol.org, Marine System Simulator, URL `http://www.marinecontrol.org/download.htm`, 2009.

J. Manley, Unmanned surface vehicles, 15 years of development, in: OCEANS 2008, 1 –4, 2008.

R. E. Kalman, A New Approach to Linear Filtering and Prediction Problems, Journal of Basic Engineering (1960) 35–45.

O. M. Faltinsen, Sea Loads on Ships and Offshore Structures, Cambridge University Press, 1990.

C. Chen, Linear Systems Theory and Design, Oxford, 3 edn., 1999.